An adaptive *hp*-refinement strategy with inexact solvers and computable guaranteed bound on the error reduction factor

Patrik Daniel, Alexandre Ern, Martin Vohralík

An adaptive *hp*-refinement strategy with inexact solvers and computable guaranteed bound on the error reduction factor*

Patrik Daniel[†‡] Alexandre Ern[‡†] Martin Vohralík[†‡]

June 9, 2019

Abstract

In this work we extend our recently proposed adaptive refinement strategy for *hp*-finite element approximations of elliptic problems by taking into account an inexact algebraic solver. Namely, on each level of refinement and on each iteration of an (arbitrary) iterative algebraic solver, we compute guaranteed a posteriori error bounds on the algebraic and the total errors in energy norm. The algebraic error is the difference between the inexact discrete solution obtained by an iterative algebraic solver and the (unavailable) exact discrete solution. On the other hand, the total error stands for the difference between the inexact discrete solution and the (unavailable) exact solution of the partial differential equation. For the algebraic error upper bound, we crucially exploit the whole nested hierarchy of *hp*-finite element spaces created by the adaptive algorithm, whereas the remaining parts of the total error upper and lower bounds are computed using the finest space only. These error bounds allow us to formulate adaptive stopping criteria for the algebraic solver ensuring that the algebraic error does not significantly contribute to the total error. Next, we use the total error bound to mark mesh vertices for refinement via Dörfler's bulk-chasing criterion. On patches associated with marked vertices only, we solve two separate primal finite element problems with homogeneous Dirichlet (Neumann) boundary conditions, which serve to decide between *h*-, *p*-, or *hp*-refinement. Altogether, we show that these ingredients lead to a computable guaranteed bound on the ratio of the total errors of the inexact approximations between successive refinements (the error reduction factor), when the stopping criteria are satisfied. Finally, in a series of numerical experiments, we investigate the practicality of the proposed adaptive solver, the accuracy of our bound on the reduction factor, and show that exponential convergence rates are achieved even in the presence of an inexact algebraic solver.

Key words: elliptic problem, finite element method, a posteriori error estimate, equilibrated flux, *hp*-adaptivity, error reduction, algebraic error

1 Introduction

The adaptive finite element method (AFEM), developed back in the 1980s [1, 2, 3, 4], is still one of the fundamental and widely used numerical methods for solving the boundary value problems arising in physics or engineering sciences. In short, it can be described as a numerical method which automatically, in an iterative fashion, adapts the employed finite element space until a sufficiently accurate approximation of the solution is obtained. For an overview and further insight, we refer the reader to work of Nochetto, Siebert and Veeser [5], and the references therein.

In the vast majority of the publications, the resulting linear systems are assumed to be solved *exactly*. However, in practical applications, including large scale numerical computations, the exact solve is not feasible in most cases; it may actually be greatly advantageous to employ an *inexact* (iterative) algebraic solver. The incorporation of an inexact algebraic solver, as an alternative to the use of (sparse) direct

*This project has received funding from the European Research Council (ERC) under the European Union's Horizon 2020 research and innovation program (grant agreement No 647134 GATIPOR).

[†]Inria, 2 rue Simone Iff, 75589 Paris, France

[‡]Université Paris-Est, CERMICS (ENPC), 77455 Marne-la-Vallée 2, France

solvers, within the AFEM framework and its rigorous analysis is rather an exception. It has been addressed by Stevenson in [6, 7], Arioli *et al.* [8, 9] for linear elliptic problems and by Holst, Szypowski, and Zhu [10], Carstensen *et al.* [11] and Gantner *et al.* [12] for nonlinear elliptic problems, all in the context of the *h*-AFEM. We also mention the work of Becker, Johnson, and Rannacher [13], where the authors deal with the issue of settling an objective stopping criterion for a multigrid iterative solver, and the work [14] where the authors devise a posteriori stopping criteria for inexact Newton methods and iterative linear solvers in the context of nonlinear diffusion PDEs.

The main goal of this manuscript is to extend the recently proposed (exact) *hp*-adaptive refinement strategy with *computable guaranteed bound on the error reduction factor* from [15] to approximate elliptic problems by taking into account an inexact algebraic iterative solver inside the *hp*-adaptive refinement loop and to drive this solver adaptively. In this work, we consider as a model problem the Poisson equation with homogeneous Dirichlet boundary conditions. Let $\Omega \subset \mathbb{R}^d$, $d = 2, 3$, be a polytopal domain (open, bounded and connected set) with a Lipschitz boundary $\partial\Omega$. The model problem in its weak form reads as follows: Seek $u \in H^1_0(\Omega)$, such that

$$(\nabla u, \nabla v) = (f, v) \qquad \forall v \in H^1_0(\Omega), \tag{1.1}$$

where $H^1_0(\Omega)$ denotes the Sobolev space of all functions in $L^2(\Omega)$ which have all their first-order weak derivatives in $L^2(\Omega)$ and a vanishing trace on $\partial\Omega$, and $(\cdot, \cdot)$ stands for the $L^2(\Omega)$ or $\left[L^2(\Omega)\right]^d$ inner product. We consider here only homogeneous Dirichlet boundary conditions for simplicity; inhomogeneous Dirichlet and Neumann conditions can be tackled in our approach as in [16]. We employ the conforming *hp*-finite element method to discretize the model problem (1.1) on a matching (no hanging nodes) simplicial mesh. The well-established paradigm of adaptive procedures, used in [15] as well, comprises at each step the four independent, but concatenated, modules, see Scheme 1. The module `SOLVE`, as already mentioned,

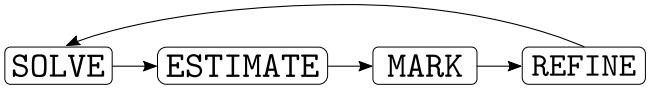

Scheme 1: Paradigm of an *hp*-adaptive loop with exact algebraic solver.

usually stands for the rather unrealistic *exact* (up to machine precision) solution of the underlying, possibly very large and/or ill-conditioned, linear algebraic problem. Thus, we opt to replace the module `SOLVE` in Scheme 1 by the module `ONE_SOLVER_STEP` coupled directly together with the module `ESTIMATE` in an adaptive fashion. This is conceptually described in Scheme 2. This scheme features an inner loop nested into an outer loop. Henceforth, we refer to the former as the inner (algebraic) loop and to the latter as the outer (*hp*) loop. Note that both loops are driven adaptively. The overall algorithm outlined in Scheme 2 is called inexact *hp*-adaptive algorithm.

Scheme 2: Paradigm of an inexact *hp*-adaptive algorithm comprising an inner (algebraic) loop and an outer (*hp*) loop; both loops are driven adaptively.

The `ONE_SOLVER_STEP` in Scheme 2 stands for performing only one (or a certain small number of) iteration(s) of the iterative solver to the resulting algebraic system. The obtained inexact solution is then immediately analyzed within the `ESTIMATE` module which now distinguishes the *algebraic error* and the *total error*. The interplay between the modules `ONE_SOLVER_STEP` and `ESTIMATE`, which is indicated by the forward and backward arrows between them in Scheme 2, corresponds to the progressive improvement of the current discrete solution by performing additional iteration(s) of the algebraic solver within module `ONE_SOLVER_STEP` with the immediate calls of module `ESTIMATE`. Our present choice of the module `ESTIMATE` is a natural extension of the developments of algebraic a posteriori error bounds via a *multilevel approach* by Papež *et al.* [17] to the present setting with variable polynomial degree. The inner (algebraic) loop is piloted by a tailored *adaptive stopping criterion*, namely, we stop at the moment when we are sure that the algebraic error lies below the total error.

The remaining two modules extend the workflow of the strategy proposed in [15]. The module `MARK` refers to applying a bulk-chasing criterion inspired by the well-known Dörfler's marking [18]; we mark mesh vertices and not simplices since we later work with some vertex-based auxiliary quantities (we also observed a smoother performance in practice when marking vertices). The module `REFINE`, including our *hp*-decision criterion, then proceeds in three steps. First, we solve two local finite element problems on each patch of simplices attached to a mesh vertex marked for refinement, with either the mesh refined or the polynomial degree increased. These conforming residual liftings allow us, in particular, to estimate the effect of applying *h*- or *p*-refinement, and lead to a partition of the set of marked vertices into two disjoint subsets, one collecting the mesh vertices flagged for *h*-refinement and the other collecting the mesh vertices flagged for *p*-refinement. The second step of the module `REFINE` uses these two subsets to flag the simplices for *h*-, *p*-, or *hp*-refinement. Finally, the third step of the module `REFINE` uses the above sets of flagged simplices to build the next simplicial mesh and the next polynomial-degree distribution.

We are particularly interested in recovering the computable guaranteed bound on the error reduction factor introduced in [15] also in the inexact setting described in Scheme 2, and for this reason our bounds are derived using various equilibrated flux reconstructions in the spirit of [14]. One of the main contributions of the present work is to show that using a properly designed stopping criterion for the algebraic solver, see Section 4.3, it is possible to compute a real number $C_{\mathrm{red}} \in [0,1]$ such that, at the end of each step of the outer (*hp*) loop in Scheme 2,

$$\|\nabla(u - u_{\ell+1})\| \leq C_{\mathrm{red}} \|\nabla(u - u_\ell)\|, \tag{1.2}$$

where u is the unknown weak solution of (1.1), u_ℓ and $u_{\ell+1}$ are its discrete inexact approximations on step ℓ, and $\ell+1$ respectively, of the outer (*hp*) loop of Scheme 2. Note that in (1.2), the inexact solution u_ℓ on the ℓ-th step of the outer (*hp*) loop is at our disposal whereas the weak solution u and the next level's inexact solution $u_{\ell+1}$ are unknown. The number C_{red} is fully computable, giving a guaranteed upper bound on the ratio of the total errors of the *inexact approximations* between two successive refinements.

The rest of this paper is organized as follows: in Section 2 we specify the discrete setting and some useful notation, in particular, concerning the inexact finite element approximation. In Section 3, we introduce the theoretical background of the a posteriori error bounds computed later within our `ESTIMATE` module. The overall description of all the modules of the proposed inexact *hp*-adaptive algorithm follows in Section 4. The result on a computable guaranteed bound on the reduction factor in the inexact setting is given in Section 5. Section 6 illustrates our theoretical findings and applicability of the proposed strategy with numerical experiments carried out on two-dimensional test cases. Finally, conclusions are drawn in Section 7.

2 Setting and notation

While using the outer (*hp*) loop of Scheme 2, a sequence of discrete finite element spaces $\{V_\ell\}_{\ell\geq 0}$, with $\ell \geq 0$ the step of the outer (*hp*) loop, is generated. We enforce the H^1_0-conformity $V_\ell \subset H^1_0(\Omega)$ for all $\ell \geq 0$ and make the following nestedness assumption:

$$V_\ell \subset V_{\ell+1}, \qquad \forall \ell \geq 0. \tag{2.1}$$

Each space V_ℓ is built up on the pair $(\mathcal{T}_\ell, \mathbf{p}_\ell)$, where $\mathcal{T}_\ell$ denotes a matching simplicial mesh of the computational domain Ω, i.e. a finite collection of (closed) non-overlapping simplices $K \in \mathcal{T}_\ell$ covering $\overline{\Omega}$ exactly and such that the intersection of two different simplices is either empty, a common vertex, a common edge, or a common face, and where the polynomial-degree distribution vector $\mathbf{p}_\ell := \{p_{\ell,K}\}_{K\in\mathcal{T}_\ell}$ assigns a degree $p_{\ell,K} \in \mathbb{N}_{\geq 1}$ to each simplex $K \in \mathcal{T}_\ell$. The conforming finite element space V_ℓ is then defined as

$$V_\ell := \mathbb{P}_{\mathbf{p}_\ell}(\mathcal{T}_\ell) \cap H^1_0(\Omega), \qquad \forall \ell \geq 0, \tag{2.2}$$

where $\mathbb{P}_{\mathbf{p}_\ell}(\mathcal{T}_\ell)$ denotes the space of piece-wise polynomials of total degree at most $p_{\ell,K}$ on each simplex $K \in \mathcal{T}_\ell$. In other words, any function $v_\ell \in V_\ell$ satisfies $v_\ell \in H^1_0(\Omega)$ and $v_\ell|_K \in \mathbb{P}_{p_{\ell,K}}(K)$ for all $K \in \mathcal{T}_\ell$, where $\mathbb{P}_p(K)$ stands for the space of all polynomials of total degree at most p on the simplex K. Let us denote by N_ℓ the dimension of the ℓ-th level space V_ℓ.

The initial coarse mesh and the initial polynomial-degree distribution $(\mathcal{T}_0, \mathbf{p}_0)$ are assumed to be given. Then, at each step of the outer (*hp*) loop $\ell \geq 0$, given the pair $(\mathcal{T}_\ell, \mathbf{p}_\ell)$, the next pair $(\mathcal{T}_{\ell+1}, \mathbf{p}_{\ell+1})$ is produced adaptively. The nestedness property (2.1) gives us two restrictions on the meshes and polynomial-degree

distributions defining the spaces V_ℓ: (i) the sequence of meshes $\{\mathcal{T}_\ell\}_{\ell\geq 0}$ needs to be *hierarchically nested*, i.e., for all $\ell \geq 1$ the mesh $\mathcal{T}_\ell$ is a refinement of $\mathcal{T}_{\ell-1}$ such that for all $K \in \mathcal{T}_\ell$, there is a unique simplex $\widetilde{K} \in \mathcal{T}_{\ell-1}$, called the parent of K, satisfying $K \subseteq \widetilde{K}$; (ii) The local polynomial degree is *locally increasing*, i.e., for all $\ell \geq 1$ and all $K \in \mathcal{T}_\ell$, $p_{\ell,K} \geq p_{\ell-1,\widetilde{K}}$, where $\widetilde{K} \in \mathcal{T}_{\ell-1}$ is the parent of K. Moreover, we assume the following standard shape-regularity property: There exists a constant $\kappa_{\mathcal{T}} > 0$ such that $\max_{K\in\mathcal{T}_\ell} h_K/\rho_K \leq \kappa_{\mathcal{T}}$ for all $\ell \geq 0$, where h_K is the diameter of K and ρ_K is the diameter of the largest ball inscribed in K.

Let us now introduce some additional useful notation. We denote by $\mathcal{V}_\ell$ the set of vertices of $\mathcal{T}_\ell$ decomposed into interior vertices $\mathcal{V}_\ell^{\text{int}}$ and vertices on the boundary $\mathcal{V}_\ell^{\text{ext}}$. For each vertex $\mathbf{a} \in \mathcal{V}_\ell$, $\ell \geq 0$, the so-called hat function $\psi_\ell^{\mathbf{a}}$ is the continuous, piecewise affine function that takes the value 1 at the vertex $\mathbf{a}$ and the value 0 at all the other vertices of $\mathcal{V}_\ell$; the function $\psi_\ell^{\mathbf{a}}$ is in V_ℓ for all $\mathbf{a} \in \mathcal{V}_\ell^{\text{int}}$. Furthermore, we consider the simplex patch $\mathcal{T}_\ell^{\mathbf{a}} \subset \mathcal{T}_\ell$ which is the collection of the simplices sharing the vertex $\mathbf{a} \in \mathcal{V}_\ell$, with $\omega_\ell^{\mathbf{a}}$ the corresponding open subdomain coinciding with the support of $\psi_\ell^{\mathbf{a}}$. Finally, for each simplex $K \in \mathcal{T}_\ell$, $\mathcal{V}_K$ denotes the set of vertices of K.

The Galerkin finite element method constructs an approximation of the weak solution u of (1.1) by solving the problem: Find $u_\ell^{\text{ex}} \in V_\ell$ such that

$$(\nabla u_\ell^{\text{ex}}, \nabla v_\ell) = (f, v_\ell) \qquad \forall v_\ell \in V_\ell. \tag{2.3}$$

The problem (2.3) is equivalent to solving the system of linear algebraic equations

$$\mathbb{A}_\ell \mathrm{U}_\ell^{\text{ex}} = \mathrm{F}_\ell, \tag{2.4}$$

where we employed ψ_ℓ^n, $1 \leq n \leq N_\ell$, the basis of the ℓ-th level space V_ℓ such that $u_\ell^{\text{ex}} := \sum_{n=1}^{N_\ell} (\mathrm{U}_\ell^{\text{ex}})_n \psi_\ell^n$. Hence, $(\mathbb{A}_\ell)_{mn} := (\nabla\psi_\ell^n, \nabla\psi_\ell^m)$ is the symmetric positive-definite stiffness matrix and $(\mathrm{F}_\ell)_m := (f, \psi_\ell^m)$ is the corresponding right-hand side vector.

However, in this work we do not assume that the algebraic system (2.4) is solved exactly (for $\ell \geq 1$). Let us denote by $\mathrm{U}_\ell \in \mathbb{R}^{N_\ell}$ an *arbitrary approximation* to the exact solution $\mathrm{U}_\ell^{\text{ex}}$ of system (2.4), corresponding to a continuous piecewise polynomial $u_\ell = \sum_{n=1}^{N_\ell} (\mathrm{U}_\ell)_n \psi_\ell^n \in V_\ell$. The *algebraic residual vector* R_ℓ associated with U_ℓ is given by

$$\mathrm{R}_\ell := \mathrm{F}_\ell - \mathbb{A}_\ell \mathrm{U}_\ell. \tag{2.5}$$

Moreover, we introduce its functional representation $\mathfrak{r}_\ell \in \mathbb{P}_{\mathbf{p}_\ell}(\mathcal{T}_\ell)$, $\mathfrak{r}_\ell|_{\partial\Omega} = 0$, i.e. a *discontinuous* polynomial of total degree at most $p_{\ell,K}$ on each $K \in \mathcal{T}_\ell$ vanishing on the boundary $\partial\Omega$ and satisfying

$$(\mathfrak{r}_\ell, \psi_\ell^n) = (\mathrm{R}_\ell)_n \qquad 1 \leq n \leq N_\ell. \tag{2.6}$$

Following Papež *et al.* [19, Section 5.1], we define $\mathfrak{r}_\ell$ in an elementwise manner by prescribing $\mathfrak{r}_\ell|_K \in \mathbb{P}_{p_{\ell,K}}(K)$, $\mathfrak{r}_\ell|_{\partial K\cap\partial\Omega} = 0$ for each simplex $K \in \mathcal{T}_\ell$ individually such that

$$(\mathfrak{r}_\ell, \psi_\ell^n)_K = \frac{(\mathrm{R}_\ell)_n}{N_\ell^n} \qquad \text{for each } \psi_\ell^n \text{ non-vanishing on } K, \tag{2.7}$$

where N_ℓ^n denotes the number of elements forming the support of the basis function ψ_ℓ^n. Note that the property (2.6) together with the definition of the algebraic system (2.4) yield the functional equivalent of algebraic relation (2.5)

$$(\mathfrak{r}_\ell, v_\ell) = (f, v_\ell) - (\nabla u_\ell, \nabla v_\ell) \qquad \forall\, v_\ell \in V_\ell. \tag{2.8}$$

3 Guaranteed total and algebraic a posteriori error bounds

Let the outer (*hp*) loop step $\ell \geq 0$ and an arbitrary approximate solution $u_\ell \in V_\ell$ be fixed. In this section we derive the a posteriori error bounds based on equilibrated flux reconstructions by local problems, see e.g. [20, 21, 22, 16, 23], adapted to the present setting of conforming *hp*-finite elements. To be more precise, we will follow the concepts from the works of Jiránek *et al.* [24], Ern and Vohralík [14], Rey *et al.* [25] and Papež *et al.* [17] in order to distinguish in the guaranteed upper bound $\eta(u_\ell, \mathcal{T}_\ell)$ on the *total energy error* $\|\nabla(u - u_\ell)\|$ two different contributions: one serving as the guaranteed upper bound on the *algebraic error* $\|\nabla(u_\ell^{\text{ex}} - u_\ell)\|$, and the rest which corresponds to the *discretization error* $\|\nabla(u - u_\ell^{\text{ex}})\|$. Finally, for

the total energy error, we also need to construct a guaranteed lower bound, so that a reliable confidence interval for the true value of $\|\nabla(u-u_\ell)\|$ is at our disposal.

The two main ingredients for the error estimators bounding from above the total and the algebraic error in energy norm are an $\mathbf{H}(\mathrm{div},\Omega)$-conforming *total flux reconstruction* and an $\mathbf{H}(\mathrm{div},\Omega)$-conforming *algebraic error flux reconstruction*:

Definition 3.1 (Total flux reconstruction $\boldsymbol{\sigma}_{\ell,\mathrm{tot}}$)**.** *We call total flux reconstruction any function $\boldsymbol{\sigma}_{\ell,\mathrm{tot}}$ constructed from the approximate solution u_ℓ satisfying*

$$\boldsymbol{\sigma}_{\ell,\mathrm{tot}} \in \mathbf{H}(\mathrm{div},\Omega), \tag{3.1a}$$

$$(\nabla\cdot\boldsymbol{\sigma}_{\ell,\mathrm{tot}}, q_\ell)_K = (f, q_\ell)_K \quad \forall K\in\mathcal{T}_\ell, \quad \forall q_\ell \in \mathbb{P}_{p_{\ell,K}}(K). \tag{3.1b}$$

Definition 3.2 (Algebraic error flux reconstruction $\boldsymbol{\sigma}_{\ell,\mathrm{alg}}$)**.** *We call algebraic error flux reconstruction any function $\boldsymbol{\sigma}_{\ell,\mathrm{alg}}$ constructed from $\mathfrak{r}_\ell$ defined in (2.7), which satisfies*

$$\boldsymbol{\sigma}_{\ell,\mathrm{alg}} \in \mathbf{H}(\mathrm{div},\Omega), \tag{3.2a}$$

$$(\nabla\cdot\boldsymbol{\sigma}_{\ell,\mathrm{alg}}, q_\ell)_K = (\mathfrak{r}_\ell, q_\ell)_K \quad \forall K\in\mathcal{T}_\ell, \quad \forall q_\ell \in \mathbb{P}_{p_{\ell,K}}(K). \tag{3.2b}$$

The requirements (3.1a) and (3.2a) above mean that both fluxes $\boldsymbol{\sigma}_{\ell,\mathrm{tot}}$ and $\boldsymbol{\sigma}_{\ell,\mathrm{alg}}$ have continuous normal traces across the mesh faces. Moreover, as we uncover in Theorem 3.3, there exists a natural decomposition of the total flux reconstruction $\boldsymbol{\sigma}_{\ell,\mathrm{tot}}$ from Definition 3.1 in the form

$$\boldsymbol{\sigma}_{\ell,\mathrm{tot}} := \boldsymbol{\sigma}_{\ell,\mathrm{alg}} + \boldsymbol{\sigma}_{\ell,\mathrm{dis}}, \tag{3.3}$$

with $\boldsymbol{\sigma}_{\ell,\mathrm{alg}}$ of Definition 3.2 and $\boldsymbol{\sigma}_{\ell,\mathrm{dis}} \in \mathbf{H}(\mathrm{div},\Omega)$, the *discretization flux reconstruction*, for which (3.2b) and (3.1b) yield

$$(\nabla\cdot\boldsymbol{\sigma}_{\ell,\mathrm{dis}}, q_\ell)_K = (f-\mathfrak{r}_\ell, q_\ell)_K \quad \forall K\in\mathcal{T}_\ell, \quad \forall q_\ell \in \mathbb{P}_{p_{\ell,K}(K)}. \tag{3.4}$$

Note that unlike in the work [17], here the properties (3.1b), (3.2b), and (3.4) are imposed on the divergences of the flux reconstructions $\boldsymbol{\sigma}_{\ell,\mathrm{tot}}$, $\boldsymbol{\sigma}_{\ell,\mathrm{alg}}$, and $\boldsymbol{\sigma}_{\ell,\mathrm{dis}}$ only in a weak sense. For piecewise polynomial source term f and uniformly distributed polynomial degrees on uniformly refined meshes, though, the requirements (3.1b), (3.2b), and (3.4) actually turn into elementwise strong equalities $\nabla\cdot\boldsymbol{\sigma}_{\ell,\mathrm{tot}} = f$, $\nabla\cdot\boldsymbol{\sigma}_{\ell,\mathrm{alg}} = \mathfrak{r}_\ell$, and $\nabla\cdot\boldsymbol{\sigma}_{\ell,\mathrm{dis}} = f-\mathfrak{r}_\ell$, where the first one captures the physical equilibrium of $\boldsymbol{\sigma}_{\ell,\mathrm{tot}}$ with the source term f. Such fluxes will indeed be locally constructed from Definitions 4.1 and 4.4 below.

Theorem 3.3 (Guaranteed upper bound on total and algebraic errors)**.** *Let $u\in H^1_0(\Omega)$ be the weak solution of the problem (1.1) and $u_\ell^{\mathrm{ex}}\in V_\ell$ be its exact finite element approximation given by (2.3). Let $u_\ell\in V_\ell$ be arbitrary. Furthermore, let $\boldsymbol{\sigma}_{\ell,\mathrm{tot}}$, $\boldsymbol{\sigma}_{\ell,\mathrm{alg}}$ be given by Definitions 3.1 and 3.2, respectively, and $\boldsymbol{\sigma}_{\ell,\mathrm{dis}}\in\mathbf{H}(\mathrm{div},\Omega)$ by (3.3). Then the following upper bound on the energy norm of the total error holds true:*

$$\|\nabla(u-u_\ell)\| \le \eta(u_\ell,\mathcal{T}_\ell) := \left\{\sum_{K\in\mathcal{T}_\ell}\eta_K^2(u_\ell)\right\}^{\frac12}, \tag{3.5a}$$

$$\eta_K(u_\ell) := \underbrace{\|\nabla u_\ell + \boldsymbol{\sigma}_{\ell,\mathrm{dis}}\|_K}_{\eta_{\mathrm{dis},K}(u_\ell)} + \underbrace{\|\boldsymbol{\sigma}_{\ell,\mathrm{alg}}\|_K}_{\eta_{\mathrm{alg},K}(u_\ell)} + \underbrace{\frac{h_K}{\pi}\|f-\nabla\cdot\boldsymbol{\sigma}_{\ell,\mathrm{tot}}\|_K}_{\eta_{\mathrm{osc},K}(u_\ell)}, \tag{3.5b}$$

and we have the upper bound on the energy norm of the algebraic error

$$\|\nabla(u_\ell^{\mathrm{ex}}-u_\ell)\| \le \eta_{\mathrm{alg}}(u_\ell,\mathcal{T}_\ell) := \left\{\sum_{K\in\mathcal{T}_\ell}\eta_{\mathrm{alg},K}^2(u_\ell)\right\}^{\frac12}. \tag{3.6}$$

Proof. The proof follows the proofs of equivalent statements in [22, 16, 17] in a straightforward way. Let us remark that it is sufficient to enforce weakly the equilibration property (3.2b), as opposed to [17] where it is enforced strongly, to prove the algebraic error upper bound (3.6). □

As discussed in, e.g. [22, Remark 3.6], the term $\eta_{\mathrm{osc},K}(u_\ell)$ represents, for all $K \in \mathcal{T}_\ell$, a local oscillation in the source datum f that, under suitable smoothness assumptions, converges to zero two orders faster than the error. The detailed description of the actual construction of the algebraic error flux reconstruction $\boldsymbol{\sigma}_{\ell,\mathrm{alg}}$ and the discretization flux reconstruction $\boldsymbol{\sigma}_{\ell,\mathrm{dis}}$, yielding the total flux reconstruction $\boldsymbol{\sigma}_{\ell,\mathrm{tot}}$, is given in Section 4.2.

Following [19, Theorem 2], the key ingredient for bounding the total energy error from below is:

Definition 3.4 (Total residual lifting $\rho_{\ell,\mathrm{tot}}$)**.** *For each vertex $\mathbf{a} \in \mathcal{V}_\ell$, let $V_\ell^{\mathbf{a}}$ be a finite-dimensional subspace of $H^1_*(\omega_\ell^{\mathbf{a}})$*

$$H^1_*(\omega_\ell^{\mathbf{a}}) := \{v \in H^1(\omega_\ell^{\mathbf{a}}), (v,1)_{\omega_\ell^{\mathbf{a}}} = 0\}, \qquad \mathbf{a} \in \mathcal{V}_\ell^{\mathrm{int}}, \tag{3.7a}$$

$$H^1_*(\omega_\ell^{\mathbf{a}}) := \{v \in H^1(\omega_\ell^{\mathbf{a}}), v = 0 \text{ on } \partial\omega_\ell^{\mathbf{a}} \cap \partial\Omega\}, \quad \mathbf{a} \in \mathcal{V}_\ell^{\mathrm{ext}}. \tag{3.7b}$$

The total residual lifting is constructed as $\rho_{\ell,\mathrm{tot}} := \sum_{\mathbf{a}\in\mathcal{V}_\ell} \psi_\ell^{\mathbf{a}} \rho_{\ell,\mathrm{tot}}^{\mathbf{a}} \in H^1_0(\Omega)$, where each vertex contribution solves the local primal finite element problem

$$\left(\nabla \rho_{\ell,\mathrm{tot}}^{\mathbf{a}}, \nabla v_\ell\right)_{\omega_\ell^{\mathbf{a}}} = (f, \psi_\ell^{\mathbf{a}} v_\ell)_{\omega_\ell^{\mathbf{a}}} - (\nabla u_\ell, \nabla(\psi_\ell^{\mathbf{a}} v_\ell))_{\omega_\ell^{\mathbf{a}}} \qquad \forall v_\ell \in V_\ell^{\mathbf{a}}. \tag{3.8}$$

Theorem 3.5 (Guaranteed lower bound on the total error)**.** *Let $u \in H^1_0(\Omega)$ be the weak solution of the problem (1.1). Let $\rho_{\ell,\mathrm{tot}}$ be associated with the approximate solution u_ℓ as in Definition 3.4. Then, the following holds true:*

$$\|\nabla(u - u_\ell)\| \geq \frac{\sum_{\mathbf{a}\in\mathcal{V}_\ell} \|\nabla \rho_{\ell,\mathrm{tot}}^{\mathbf{a}}\|^2_{\omega_\ell^{\mathbf{a}}}}{\|\nabla \rho_{\ell,\mathrm{tot}}\|} =: \mu(u_\ell). \tag{3.9}$$

Proof. For completeness, we include the proof following some basic observations from [26, Section 5.1] or [27, Section 4.1.1] and the concrete construction in [19, Theorem 2]. As $\rho_{\ell,\mathrm{tot}} \in H^1_0(\Omega)$ by construction, employing the definition of the energy norm $\|\nabla(u - u_\ell)\|$, we have

$$\begin{aligned}
\|\nabla(u - u_\ell)\| &= \sup_{v\in H^1_0(\Omega), \|\nabla v\|=1} (\nabla(u - u_\ell), \nabla v) \\
&\geq \frac{1}{\|\nabla \rho_{\ell,\mathrm{tot}}\|} (\nabla(u - u_\ell), \nabla \rho_{\ell,\mathrm{tot}}) \\
&= \frac{1}{\|\nabla \rho_{\ell,\mathrm{tot}}\|} \sum_{\mathbf{a}\in\mathcal{V}_\ell} (\nabla(u - u_\ell), \nabla(\psi_\ell^{\mathbf{a}} \rho_{\ell,\mathrm{tot}}^{\mathbf{a}}))_{\omega_\ell^{\mathbf{a}}} \\
&= \frac{1}{\|\nabla \rho_{\ell,\mathrm{tot}}\|} \sum_{\mathbf{a}\in\mathcal{V}_\ell} \left\{ \left(f, \psi_\ell^{\mathbf{a}} \rho_{\ell,\mathrm{tot}}^{\mathbf{a}}\right)_{\omega_\ell^{\mathbf{a}}} - \left(\nabla u_\ell, \nabla(\psi_\ell^{\mathbf{a}} \rho_{\ell,\mathrm{tot}}^{\mathbf{a}})\right)_{\omega_\ell^{\mathbf{a}}} \right\} \\
&= \frac{1}{\|\nabla \rho_{\ell,\mathrm{tot}}\|} \sum_{\mathbf{a}\in\mathcal{V}_\ell} \|\nabla \rho_{\ell,\mathrm{tot}}^{\mathbf{a}}\|^2_{\omega_\ell^{\mathbf{a}}},
\end{aligned}$$

where we used the fact that $\psi_\ell^{\mathbf{a}} \rho_{\ell,\mathrm{tot}}^{\mathbf{a}} \in H^1_0(\omega_\ell^{\mathbf{a}})$ for all vertices $\mathbf{a} \in \mathcal{V}_\ell$ and the definition (3.8) of $\rho_{\ell,\mathrm{tot}}^{\mathbf{a}}$. □

4 The inexact *hp*-adaptive algorithm

In this section we present the modules `ONE_SOLVER_STEP`, `ESTIMATE`, `MARK`, and `REFINE` used in Scheme 2. We recall that $\ell \geq 0$ denotes the step of the outer (hp) loop.

4.1 The module `ONE_SOLVER_STEP`

First, let the current step of the outer (hp) loop be $\ell = 0$. Note that at this stage the nested sequence of spaces characterized by (2.1) and (2.2) contains only the initial H^1_0-conforming finite element space V_0. This represents a special case where the module `ONE_SOLVER_STEP` takes as input only the space V_0 and sets the output function $u_0 \in V_0$ directly to be the exact solution of (2.3); here the corresponding (still small) linear algebraic problem (2.4) is considered to be solved exactly.

Otherwise, for the step $\ell \geq 1$, the module `ONE_SOLVER_STEP` may and in most cases will be called several times due to the coupling with the `ESTIMATE` module (cf. Scheme 2). Let $P_{\ell-1}^{\ell} : V_{\ell-1} \to V_{\ell}$ be a canonical prolongation operator between the consecutive nested finite element spaces. Before the initial call of `ONE_SOLVER_STEP` at step ℓ, we initialize the ℓ-th level approximation $u_\ell \in V_\ell$ of the exact finite element solution u_ℓ^{ex}, by setting $u_\ell := P_{\ell-1}^{\ell} u_{\ell-1}$. This corresponds to setting the initial guess for the algebraic solver. The module `ONE_SOLVER_STEP` for $\ell \geq 1$ takes as input not only the space V_ℓ, but also the current approximation u_ℓ which is in turn improved and returned as the output of the module. Here, by the improvement of u_ℓ, we mean applying one or a given small number of steps of the given iterative algebraic solver to the system (2.4) assembled within the initial call of `ONE_SOLVER_STEP` at the outer (*hp*) loop step ℓ.

The quality of the output u_ℓ is then assessed by the module `ESTIMATE` and if necessary, see Section 4.3, u_ℓ is passed again as an input to the successive call of the module `ONE_SOLVER_STEP`.

4.2 The module `ESTIMATE`

The module `ESTIMATE` crucially relies on the theoretical developments of Section 3. It takes as input the current approximation u_ℓ to the exact finite element solution u_ℓ^{ex}, computes the corresponding flux reconstructions $\boldsymbol{\sigma}_{\ell,\mathrm{alg}}$, $\boldsymbol{\sigma}_{\ell,\mathrm{dis}}$, $\boldsymbol{\sigma}_{\ell,\mathrm{tot}}$ and the total residual lifting $\rho_{\ell,\mathrm{tot}}$ defined in Section 3, and finally outputs a collection of local error indicators $\{\eta_{\mathrm{alg},K}(u_\ell), \eta_{\mathrm{dis},K}(u_\ell), \eta_{\mathrm{osc},K}(u_\ell)\}_{K\in\mathcal{T}_\ell}$ together with the lower bound $\mu(u_\ell)$ defined in Theorems 3.3 and 3.5, respectively. In what follows, we outline all the necessary details concerning the actual construction of the flux reconstructions $\boldsymbol{\sigma}_{\ell,\mathrm{alg}}$ and $\boldsymbol{\sigma}_{\ell,\mathrm{dis}}$, hence also their sum $\boldsymbol{\sigma}_{\ell,\mathrm{tot}}$, and the lifting $\rho_{\ell,\mathrm{tot}}$. Once they are all properly constructed, the local error indicators $\eta_{*,K}(u_\ell)$, $* = \mathrm{dis}, \mathrm{alg}, \mathrm{osc}$, of (3.5b) and $\mu(u_\ell)$ defined in (3.9) are evaluated.

4.2.1 Multilevel construction of algebraic error flux reconstruction $\boldsymbol{\sigma}_{\ell,\mathrm{alg}}$

In order to obtain the algebraic error flux reconstruction $\boldsymbol{\sigma}_{\ell,\mathrm{alg}}$ of Definition 3.2, we use the multilevel approach introduced by Papež *et al.* in [17]. We extend it here to the present conforming *hp*-finite element setting. The multilevel approach is a natural choice, especially in the present adaptive framework, where for the current space V_ℓ, built up on the pair $(\mathcal{T}_\ell, \mathbf{p}_\ell)$, the hierarchy of its nested finite element subspaces $\{V_j\}_{0\leq j<\ell}$, together with the meshes and polynomial degree distributions $\{(\mathcal{T}_j, \mathbf{p}_j)\}_{0\leq j<\ell}$, are readily at hand from the previous steps of the outer (*hp*) loop. We will refer to the mesh levels 0 and ℓ as the coarsest and the finest level, respectively.

Firstly, following [17], for the algebraic residual $\mathfrak{r}_\ell \in \mathbb{P}_{\mathbf{p}_\ell}(\mathcal{T}_\ell)$ given by (2.7) we introduce the *coarsest-level Riesz representer* $\varphi_{0,\mathrm{alg}} \in V_0$

$$(\nabla\varphi_{0,\mathrm{alg}}, \nabla v_0) = (\mathfrak{r}_\ell, v_0) \quad \forall v_0 \in V_0. \tag{4.1}$$

For each $\mathbf{a} \in \mathcal{V}_j$, $0 \leq j \leq \ell$, recall the definition of a simplex patch $\mathcal{T}_j^{\mathbf{a}}$ with the corresponding subdomain $\omega_j^{\mathbf{a}}$. In addition, let us introduce for each coarse vertex $\mathbf{a} \in \mathcal{V}_{j-1}$, $1 \leq j \leq \ell$, a simplex patch $\mathcal{T}_{j,j-1}^{\mathbf{a}}$ of all the next finer level simplices $K \in \mathcal{T}_j$ such that $K \subset \omega_{j-1}^{\mathbf{a}}$, cf. Figure 1, and the local polynomial degree $p_{\mathbf{a}}^{\mathrm{alg}} := \max_{K\in\mathcal{T}_{j,j-1}^{\mathbf{a}}} p_{j,K}$ (any other choice so that $p_{\mathbf{a}}^{\mathrm{alg}} \geq \max_{K\in\mathcal{T}_{j,j-1}^{\mathbf{a}}} p_{j,K}$ can also be considered).

Let the mesh level $1 \leq j \leq \ell$ be fixed together with the vertex from the next coarser mesh $\mathbf{a} \in \mathcal{V}_{j-1}$. We define the local p-th order Raviart–Thomas–Nédélec space on the subdomain $\omega_{j-1}^{\mathbf{a}}$ with the mesh induced by the next finer mesh $\mathcal{T}_j$ by

$$\mathbf{RTN}_p\left(\omega_{j-1}^{\mathbf{a}}\right) = \{\mathbf{v}_j \in \mathbf{H}(\mathrm{div}, \omega_{j-1}^{\mathbf{a}});\, \mathbf{v}_j|_K \in \mathbf{RTN}_p(K), \quad \forall K \in \mathcal{T}_{j,j-1}^{\mathbf{a}}\}, \tag{4.2}$$

where $\mathbf{RTN}_p(K) = [\mathbb{P}_p(K)]^d + \mathbb{P}_p(K)\mathbf{x}$ is the usual p-th order Raviart–Thomas–Nédélec space (cf. [28, 29]) on a simplex $K \in \mathcal{T}_j$. Furthermore, we consider the pair of local mixed finite element spaces $(\mathbf{V}_{j,j-1}^{\mathbf{a}}, Q_{j,j-1}^{\mathbf{a}})$ which are defined by

$$\begin{aligned} &\mathbf{V}_{j,j-1}^{\mathbf{a}} := \{\mathbf{v}_j \in \mathbf{RTN}_{p_{\mathbf{a}}^{\mathrm{alg}}}\left(\omega_{j-1}^{\mathbf{a}}\right);\, \mathbf{v}_j\cdot\mathbf{n}_{\omega_{j-1}^{\mathbf{a}}} = 0 \text{ on } \partial\omega_{j-1}^{\mathbf{a}}\},\\ &Q_{j,j-1}^{\mathbf{a}} := \{q_j \in \mathbb{P}_{p_{\mathbf{a}}^{\mathrm{alg}}}\left(\mathcal{T}_{j,j-1}^{\mathbf{a}}\right);\, (q_j, 1)_{\omega_{j-1}^{\mathbf{a}}} = 0\}, \end{aligned} \qquad \text{if } \mathbf{a} \in \mathcal{V}_{j-1}^{\mathrm{int}}, \tag{4.3a}$$

$$\begin{aligned} &\mathbf{V}_{j,j-1}^{\mathbf{a}} := \{\mathbf{v}_j \in \mathbf{RTN}_{p_{\mathbf{a}}^{\mathrm{alg}}}\left(\omega_{j-1}^{\mathbf{a}}\right);\, \mathbf{v}_j\cdot\mathbf{n}_{\omega_{j-1}^{\mathbf{a}}} = 0 \text{ on } \partial\omega_{j-1}^{\mathbf{a}} \setminus \partial\Omega\},\\ &Q_{j,j-1}^{\mathbf{a}} := \mathbb{P}_{p_{\mathbf{a}}^{\mathrm{alg}}}\left(\mathcal{T}_{j,j-1}^{\mathbf{a}}\right), \end{aligned} \qquad \text{if } \mathbf{a} \in \mathcal{V}_{j-1}^{\mathrm{ext}}, \tag{4.3b}$$

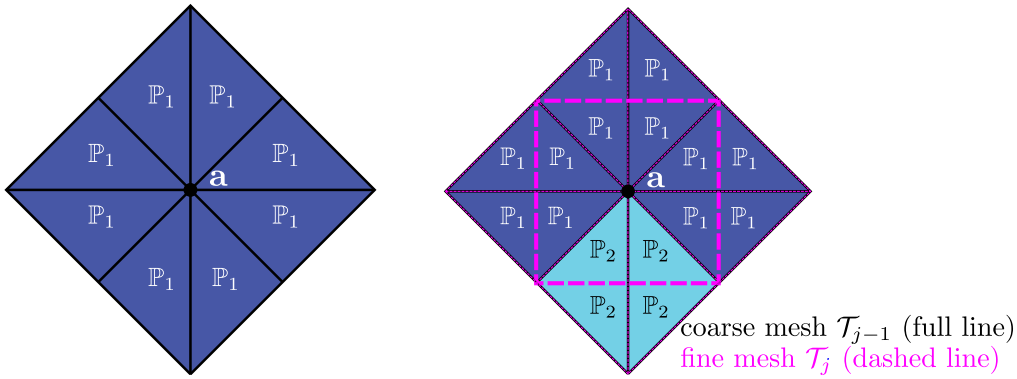

Figure 1: Patches of simplices $\mathcal{T}^{\mathbf{a}}_{j-1}$ (*left*) and $\mathcal{T}^{\mathbf{a}}_{j,j-1}$ (*right*) in the subdomain $\omega^{\mathbf{a}}_{j-1}$ around a coarse vertex $\mathbf{a} \in \mathcal{T}_{j-1}$ together with the corresponding polynomial degree distributions. Note that in this case, the local polynomial degree $p^{\mathrm{alg}}_{\mathbf{a}} = 2$.

where $\mathbf{n}_{\omega^{\mathbf{a}}_{j-1}}$ denotes the unit outward normal to $\omega^{\mathbf{a}}_{j-1}$. For an interior vertex $\mathbf{a} \in \mathcal{V}^{\mathrm{int}}_{j-1}$, the degrees of freedom of the spaces $\mathbf{V}^{\mathbf{a}}_{j,j-1}$ and $Q^{\mathbf{a}}_{j,j-1}$ with the local polynomial degree $p^{\mathrm{alg}}_{\mathbf{a}} = 2$ are illustrated in Figure 2.

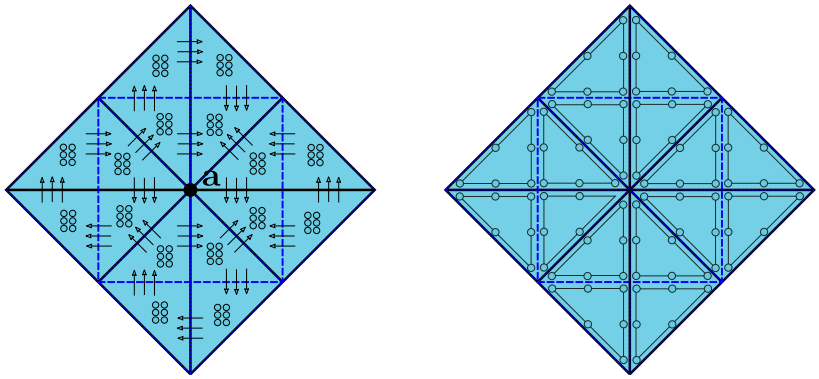

Figure 2: Degrees of freedom of the local mixed finite element spaces $\mathbf{V}^{\mathbf{a}}_{j,j-1}$ (*left*, arrows and bullets) and $Q^{\mathbf{a}}_{j,j-1}$ (*right*, bullets) with $p^{\mathrm{alg}}_{\mathbf{a}} = 2$; interior vertex $\mathbf{a} \in \mathcal{V}^{\mathrm{int}}_{j-1}$. On the right, leaving out one degree of freedom of the broken space $\mathbb{P}_{p^{\mathrm{alg}}_{\mathbf{a}}}\left(\mathcal{T}^{\mathbf{a}}_{j,j-1}\right)$ corresponds to the zero mean value constraint posed on the functions in $Q^{\mathbf{a}}_{j,j-1}$. The underlying mesh and the choice of $p^{\mathrm{alg}}_{\mathbf{a}}$ correspond to the simplex patch $\mathcal{T}^{\mathbf{a}}_{j,j-1}$ from Figure 1.

Once the coarsest-level Riesz representer $\varphi_{0,\mathrm{alg}}$ of (4.1) is computed, the algebraic error flux reconstruction $\boldsymbol{\sigma}_{\ell,\mathrm{alg}}$ is constructed by solving the local dual mixed finite element problems on simplex patches $\mathcal{T}^{\mathbf{a}}_{j,j-1}$ around the coarse vertices $\mathbf{a} \in \mathcal{V}_{j-1}$, starting from $j = 1$ and up to the current finest level $j = \ell$:

Definition 4.1 (Construction of $\boldsymbol{\sigma}_{\ell,\mathrm{alg}}$)**.** *Let $u_\ell \in V_\ell$ be arbitrary. The algebraic error flux reconstruction $\boldsymbol{\sigma}_{\ell,\mathrm{alg}}$ is constructed as*

$$\boldsymbol{\sigma}_{\ell,\mathrm{alg}} := \sum_{j=1}^{\ell} \sum_{\mathbf{a} \in \mathcal{V}_{j-1}} \boldsymbol{\sigma}^{\mathbf{a}}_{j,\mathrm{alg}}, \tag{4.4}$$

where:

- *On level $j = 1$, for each vertex $\mathbf{a} \in \mathcal{V}_0$, $(\boldsymbol{\sigma}^{\mathbf{a}}_{1,\mathrm{alg}}, \gamma^{\mathbf{a}}_1) \in \mathbf{V}^{\mathbf{a}}_{1,0} \times Q^{\mathbf{a}}_{1,0}$ solves*

$$\left(\boldsymbol{\sigma}^{\mathbf{a}}_{1,\mathrm{alg}}, \mathbf{v}_1\right)_{\omega^{\mathbf{a}}_0} - \left(\gamma^{\mathbf{a}}_1, \nabla{\cdot}\mathbf{v}_1\right)_{\omega^{\mathbf{a}}_0} = 0 \qquad \forall \mathbf{v}_1 \in \mathbf{V}^{\mathbf{a}}_{1,0}, \tag{4.5a}$$

$$\left(\nabla{\cdot}\boldsymbol{\sigma}^{\mathbf{a}}_{1,\mathrm{alg}}, q_1\right)_{\omega^{\mathbf{a}}_0} = \left(\mathfrak{r}_\ell \psi^{\mathbf{a}}_0 - \nabla\varphi_{0,\mathrm{alg}}{\cdot}\nabla\psi^{\mathbf{a}}_0, q_1\right)_{\omega^{\mathbf{a}}_0} \quad \forall q_1 \in Q^{\mathbf{a}}_{1,0}; \tag{4.5b}$$

or, equivalently,

$$\boldsymbol{\sigma}^{\mathbf{a}}_{1,\mathrm{alg}} := \operatorname*{arg\,min}_{\mathbf{v}_1\in\mathbf{V}^{\mathbf{a}}_{1,0},\nabla\cdot\mathbf{v}_1=\Pi_{Q^{\mathbf{a}}_{1,0}}\left(\mathfrak{r}_\ell\psi^{\mathbf{a}}_0-\nabla\varphi_{0,\mathrm{alg}}\cdot\nabla\psi^{\mathbf{a}}_0\right)} \|\mathbf{v}_1\|_{\omega^{\mathbf{a}}_0}. \tag{4.6}$$

- *On level $2\le j\le \ell$, for each vertex $\mathbf{a}\in\mathcal{V}_{j-1}$, $(\boldsymbol{\sigma}^{\mathbf{a}}_{j,\mathrm{alg}},\gamma^{\mathbf{a}}_j)\in\mathbf{V}^{\mathbf{a}}_{j,j-1}\times Q^{\mathbf{a}}_{j,j-1}$ solves*

$$\left(\boldsymbol{\sigma}^{\mathbf{a}}_{j,\mathrm{alg}},\mathbf{v}_j\right)_{\omega^{\mathbf{a}}_{j-1}}-\left(\gamma^{\mathbf{a}}_j,\nabla\cdot\mathbf{v}_j\right)_{\omega^{\mathbf{a}}_{j-1}}=0 \qquad \forall\mathbf{v}_j\in\mathbf{V}^{\mathbf{a}}_{j,j-1}, \tag{4.7a}$$

$$\left(\nabla\cdot\boldsymbol{\sigma}^{\mathbf{a}}_{j,\mathrm{alg}},q_j\right)_{\omega^{\mathbf{a}}_{j-1}}=\left(\mathfrak{r}_\ell\psi^{\mathbf{a}}_{j-1}-\sum_{i=1}^{j-1}\psi^{\mathbf{a}}_{j-1}\nabla\cdot\boldsymbol{\sigma}_{i,\mathrm{alg}},q_j\right)_{\omega^{\mathbf{a}}_{j-1}} \qquad \forall q_j\in Q^{\mathbf{a}}_{j,j-1}; \tag{4.7b}$$

where we set $\boldsymbol{\sigma}_{i,\mathrm{alg}}:=\sum_{\mathbf{a}\in\mathcal{V}_{i-1}}\boldsymbol{\sigma}^{\mathbf{a}}_{i,\mathrm{alg}}$, for $1\le i\le j-1$. Equivalently, problem (4.7) can be restated as

$$\boldsymbol{\sigma}^{\mathbf{a}}_{j,\mathrm{alg}} := \operatorname*{arg\,min}_{\mathbf{v}_j\in\mathbf{V}^{\mathbf{a}}_{j,j-1},\nabla\cdot\mathbf{v}_j=\Pi_{Q^{\mathbf{a}}_{j,j-1}}\left(\mathfrak{r}_\ell\psi^{\mathbf{a}}_{j-1}-\sum_{i=1}^{j-1}\psi^{\mathbf{a}}_{j-1}\nabla\cdot\boldsymbol{\sigma}_{i,\mathrm{alg}}\right)} \|\mathbf{v}_j\|_{\omega^{\mathbf{a}}_{j-1}}. \tag{4.8}$$

Here, each vertex contribution $\boldsymbol{\sigma}^{\mathbf{a}}_{j,\mathrm{alg}}$, $1\le j\le\ell$, is extended by zero outside its initial domain of definition.

Note that the Neumann compatibility condition for problem (4.5) is satisfied for all $\mathbf{a}\in\mathcal{V}^{\mathrm{int}}_0$ due to the definition of $\varphi_{0,\mathrm{alg}}$ (take $v_0=\psi^{\mathbf{a}}_0$ as a test function in (4.1)). Thus (4.5b) is satisfied for all the test functions from $\mathbb{P}_{p^{\mathrm{alg}}_{\mathbf{a}}}(\mathcal{T}^{\mathbf{a}}_{1,0})$, not only those with zero mean value. Due to the discontinuous nature of this broken polynomial space and the fact that for each $K\in\mathcal{T}_1$, with the parent element $\widetilde{K}\in\mathcal{T}_0$, $p_{1,K}\le\min_{\mathbf{a}\in\mathcal{V}_{\widetilde{K}}}p^{\mathrm{alg}}_{\mathbf{a}}$, we have

$$\begin{aligned}\left(\nabla\cdot\boldsymbol{\sigma}_{1,\mathrm{alg}},q_1\right)_K&=\sum_{\mathbf{a}\in\mathcal{V}_{\widetilde{K}}}\left(\nabla\cdot\boldsymbol{\sigma}^{\mathbf{a}}_{1,\mathrm{alg}},q_1\right)_K=\sum_{\mathbf{a}\in\mathcal{V}_{\widetilde{K}}}\left(\mathfrak{r}_\ell\psi^{\mathbf{a}}_0-\nabla\varphi_{0,\mathrm{alg}}\cdot\nabla\psi^{\mathbf{a}}_0,q_1\right)_K\\&=\left(\mathfrak{r}_\ell,q_1\right)_K\quad\forall K\in\mathcal{T}_1\quad\forall q_1\in\mathbb{P}_{p_{1,K}}(K),\end{aligned} \tag{4.9}$$

where we employed the partition of unity via $\sum_{\mathbf{a}\in\mathcal{V}_{\widetilde{K}}}\psi^{\mathbf{a}}_0|_K=1|_K$. At level $j=2$, for each interior vertex $\mathbf{a}\in\mathcal{V}^{\mathrm{int}}_1$, the Neumann compatibility condition for problem (4.7) $(\mathfrak{r}_\ell-\nabla\cdot\boldsymbol{\sigma}_{1,\mathrm{alg}},\psi^{\mathbf{a}}_1)_{\omega^{\mathbf{a}}_1}=0$ is a direct consequence of (4.9), since $\psi^{\mathbf{a}}_1|_K\in\mathbb{P}_{p_{1,K}}(K)$ for each $K\in\mathcal{T}^{\mathbf{a}}_1$. Thus, similarly to (4.5b) also (4.7b), so far only at level $j=2$, is satisfied for all the test functions from $\mathbb{P}_{p^{\mathrm{alg}}_{\mathbf{a}}}(\mathcal{T}^{\mathbf{a}}_{2,1})$ without any zero-mean value restriction. Then, similarly to (4.9), we use the discontinuous nature of the broken space $\mathbb{P}_{p^{\mathrm{alg}}_{\mathbf{a}}}(\mathcal{T}^{\mathbf{a}}_{2,1})$, our choice of local polynomial degrees $p^{\mathrm{alg}}_{\mathbf{a}}$ in the definition of the spaces (4.3), for each vertex $\mathbf{a}\in\mathcal{V}_1$, such that $p_{2,K}\le\min_{\mathbf{a}\in\mathcal{V}_{\widetilde{K}}}p^{\mathrm{alg}}_{\mathbf{a}}$, for each $K\in\mathcal{T}_2$ with the parent element $\widetilde{K}\in\mathcal{T}_1$, and the partition of unity via $\sum_{\mathbf{a}\in\mathcal{V}_{\widetilde{K}}}\psi^{\mathbf{a}}_1|_K=1$ to obtain

$$\left(\mathfrak{r}_\ell-\sum_{i=1}^{2}\nabla\cdot\boldsymbol{\sigma}_{i,\mathrm{alg}},q_2\right)_K=0\quad\forall K\in\mathcal{T}_2\quad\forall q_2\in\mathbb{P}_{p_{2,K}}(K). \tag{4.10}$$

Property (4.10) in turn yields the Neumann compatibility condition on the third level. Progressing successively, at the remaining levels $3\le j\le\ell-1$, we always have the property

$$\left(\mathfrak{r}_\ell-\sum_{i=1}^{j}\nabla\cdot\boldsymbol{\sigma}_{i,\mathrm{alg}},q_j\right)_K=0\quad\forall K\in\mathcal{T}_j\quad\forall q_j\in\mathbb{P}_{p_{j,K}}(K), \tag{4.11}$$

yielding the Neumann compatibility condition on the next level $j+1$, thus (4.7b) is satisfied for all the test functions from the broken polynomial space $\mathbb{P}_{p^{\mathrm{alg}}_{\mathbf{a}}}(\mathcal{T}^{\mathbf{a}}_{j,j-1})$, for each $\mathbf{a}\in\mathcal{V}_{j-1}$, $2\le j\le\ell$. Furthermore, as a result of the Neumann compatibility condition on the finest level, on each finest simplex $K\in\mathcal{T}_\ell$, the sum of local contributions $\sum_{\mathbf{a}\in\mathcal{V}_{\ell-1}}\boldsymbol{\sigma}^{\mathbf{a}}_{\ell,\mathrm{alg}}$ admits the following property:

$$\left(\sum_{\mathbf{a}\in\mathcal{V}_{\ell-1}}\nabla\cdot\boldsymbol{\sigma}^{\mathbf{a}}_{\ell,\mathrm{alg}},q_\ell\right)_K=\sum_{\mathbf{a}\in\mathcal{V}_{\widetilde{K}}}\left(\nabla\cdot\boldsymbol{\sigma}^{\mathbf{a}}_{\ell,\mathrm{alg}},q_\ell\right)_K=\left(\mathfrak{r}_\ell-\sum_{i=1}^{\ell-1}\nabla\cdot\boldsymbol{\sigma}_{i,\mathrm{alg}},q_\ell\right)_K\qquad\forall q_\ell\in\mathbb{P}_{p_{\ell,K}}(K). \tag{4.12}$$

Lemma 4.2 (Properties of $\boldsymbol{\sigma}_{\ell,\mathrm{alg}}$)**.** *The algebraic error flux reconstruction $\boldsymbol{\sigma}_{\ell,\mathrm{alg}}$ constructed in Definition 4.1 satisfies the properties of Definition 3.2.*

Proof. For all $1 \le j \le \ell$, each local contribution $\boldsymbol{\sigma}^{\mathbf{a}}_{j,\mathrm{alg}} \in \mathbf{H}(\mathrm{div}, \omega^{\mathbf{a}}_{j-1})$, $\mathbf{a} \in \mathcal{V}_{j-1}$, by construction. Imposing the homogeneous Neumann boundary conditions in the definition of the local spaces (4.3) and extending by zero outside of $\omega^{\mathbf{a}}_{j-1}$ then give the overall $\mathbf{H}(\mathrm{div}, \Omega)$-conformity (3.2a) of $\boldsymbol{\sigma}_{\ell,\mathrm{alg}}$ as it is defined by (4.4). Then, splitting the sum in the definition (4.4) in combination with the property (4.12) yields for each $K \in \mathcal{T}_\ell$,

$$(\nabla\cdot\boldsymbol{\sigma}_{\ell,\mathrm{alg}}, q_\ell)_K = \left(\sum_{\mathbf{a}\in\mathcal{V}_{\ell-1}} \nabla\cdot\boldsymbol{\sigma}^{\mathbf{a}}_{\ell,\mathrm{alg}} + \sum_{i=1}^{\ell-1} \nabla\cdot\boldsymbol{\sigma}_{i,\mathrm{alg}}, q_\ell \right)_K = (\mathfrak{r}_\ell, q_\ell)_K \quad \forall q_\ell \in \mathbb{P}_{p_{\ell,K}}(K).$$

Hence, the algebraic error flux reconstruction $\boldsymbol{\sigma}_{\ell,\mathrm{alg}}$ satisfies (3.2b). □

Remark 4.3 (Comparison with previous developments)**.** *The local problems in Definition 4.1 differ from those of* [17, Definition 6.3] *in two aspects:* (i) *the local spaces on each simplex patch are assigned a specific polynomial degree along the lines of* [15, 16]*;* (ii) *the right-hand sides of the local problems* (4.7)*, namely the divergence constraints in* (4.7b)*, differ from their counterparts in* [17, Definition 6.3]*. In particular, the first level algebraic error flux reconstruction $\boldsymbol{\sigma}_{1,\mathrm{alg}}$ is now successively corrected on the finer levels without the need of introducing the L^2-orthogonal projections onto global coarser spaces, which is not suitable anymore because of the possibly varying polynomial degrees $p^{\mathrm{alg}}_{\mathbf{a}}$ across the neighboring patches.*

4.2.2 Construction of the discretization flux reconstruction $\boldsymbol{\sigma}_{\ell,\mathrm{dis}}$

Next, we present the details on the actual construction of the $\mathbf{H}(\mathrm{div}, \Omega)$-conforming discretization flux reconstruction $\boldsymbol{\sigma}_{\ell,\mathrm{dis}}$. Similarly to the above construction of $\boldsymbol{\sigma}_{\ell,\mathrm{alg}}$, we construct $\boldsymbol{\sigma}_{\ell,\mathrm{dis}}$ locally via mixed finite element solves, but this time only on the finest simplex patches $\mathcal{T}^{\mathbf{a}}_\ell$ around the finest mesh vertices $\mathbf{a} \in \mathcal{V}_\ell$. Namely, we follow the approach of [17, Definition 7.1], [19, Sec. 4.4], and [14, Definition 6.9] adapted to the present setting with varying polynomial degree. For each $\mathbf{a} \in \mathcal{V}_\ell$, we consider the local polynomial degree $is := \max_{K\in\mathcal{T}^{\mathbf{a}}_\ell} p_{\ell,K}$ (again any other choice so that $is \ge \max_{K\in\mathcal{T}^{\mathbf{a}}_\ell} p_{\ell,K}$ can be employed). For a fixed finest vertex $\mathbf{a} \in \mathcal{V}_\ell$, let

$$\mathbf{RTN}_p(\omega^{\mathbf{a}}_\ell) = \{\mathbf{v}_\ell \in \mathbf{H}(\mathrm{div}, \omega^{\mathbf{a}}_\ell);\ \mathbf{v}_\ell|_K \in \mathbf{RTN}_p(K), \quad \forall K \in \mathcal{T}^{\mathbf{a}}_\ell\}. \tag{4.13}$$

Then, we define the local spaces with homogeneous Neumann boundary condition

$$\begin{aligned} &\mathbf{V}^{\mathbf{a}}_\ell := \{\mathbf{v}_\ell \in \mathbf{RTN}_{is}(\omega^{\mathbf{a}}_\ell);\ \mathbf{v}_\ell\cdot\mathbf{n}_{\omega^{\mathbf{a}}_\ell} = 0 \text{ on } \partial\omega^{\mathbf{a}}_\ell\},\\ &Q^{\mathbf{a}}_\ell := \{q_\ell \in \mathbb{P}_{is}(\mathcal{T}^{\mathbf{a}}_\ell);\ (q_\ell, 1)_{\omega^{\mathbf{a}}_\ell} = 0\}, \end{aligned} \qquad \text{if } \mathbf{a} \in \mathcal{V}^{\mathrm{int}}_\ell, \tag{4.14a}$$

$$\begin{aligned} &\mathbf{V}^{\mathbf{a}}_\ell := \{\mathbf{v}_\ell \in \mathbf{RTN}_{is}(\omega^{\mathbf{a}}_\ell);\ \mathbf{v}_\ell\cdot\mathbf{n}_{\omega^{\mathbf{a}}_\ell} = 0 \text{ on } \partial\omega^{\mathbf{a}}_\ell \setminus \partial\Omega\},\\ &Q^{\mathbf{a}}_\ell := \mathbb{P}_{is}(\mathcal{T}^{\mathbf{a}}_\ell), \end{aligned} \qquad \text{if } \mathbf{a} \in \mathcal{V}^{\mathrm{ext}}_\ell, \tag{4.14b}$$

with $\mathbf{n}_{\omega^{\mathbf{a}}_\ell}$ denoting the unit outward normal to $\omega^{\mathbf{a}}_\ell$.

Definition 4.4 (Construction of $\boldsymbol{\sigma}_{\ell,\mathrm{dis}}$)**.** *Let $u_\ell \in V_\ell$ be the approximation used in Definition 4.1. We construct the discretization flux reconstruction $\boldsymbol{\sigma}_{\ell,\mathrm{dis}}$ as*

$$\boldsymbol{\sigma}_{\ell,\mathrm{dis}} := \sum_{\mathbf{a}\in\mathcal{V}_\ell} \boldsymbol{\sigma}^{\mathbf{a}}_{\ell,\mathrm{dis}}, \tag{4.15}$$

where, for each vertex $\mathbf{a} \in \mathcal{V}_\ell$, $(\boldsymbol{\sigma}^{\mathbf{a}}_{\ell,\mathrm{dis}}, \gamma^{\mathbf{a}}_\ell) \in \mathbf{V}^{\mathbf{a}}_\ell \times Q^{\mathbf{a}}_\ell$ solves

$$(\boldsymbol{\sigma}^{\mathbf{a}}_{\ell,\mathrm{dis}}, \mathbf{v}_\ell)_{\omega^{\mathbf{a}}_\ell} - (\gamma^{\mathbf{a}}_\ell, \nabla\cdot\mathbf{v}_\ell)_{\omega^{\mathbf{a}}_\ell} = -(\psi^{\mathbf{a}}_\ell \nabla u_\ell, \mathbf{v}_\ell)_{\omega^{\mathbf{a}}_\ell} \qquad \forall \mathbf{v}_\ell \in \mathbf{V}^{\mathbf{a}}_\ell, \tag{4.16a}$$

$$(\nabla\cdot\boldsymbol{\sigma}^{\mathbf{a}}_{\ell,\mathrm{dis}}, q_\ell)_{\omega^{\mathbf{a}}_\ell} = (f\psi^{\mathbf{a}}_\ell - \nabla u_\ell\cdot\nabla\psi^{\mathbf{a}}_\ell - \mathfrak{r}_\ell\psi^{\mathbf{a}}_\ell, q_\ell)_{\omega^{\mathbf{a}}_\ell} \quad \forall q_\ell \in Q^{\mathbf{a}}_\ell, \tag{4.16b}$$

and where $\boldsymbol{\sigma}^{\mathbf{a}}_{\ell,\mathrm{dis}}$ is extended by zero outside $\omega^{\mathbf{a}}_\ell$.

The Neumann compatibility condition for problem (4.16) is satisfied for all $\mathbf{a} \in \mathcal{V}_\ell^{\text{int}}$ as a direct consequence of (2.8).

Lemma 4.5 (Properties of $\boldsymbol{\sigma}_{\ell,\text{dis}}$)**.** *The discretization flux reconstruction $\boldsymbol{\sigma}_{\ell,\text{dis}}$ from Definition 4.4 belongs to $\mathbf{H}(\text{div},\Omega)$ and on each simplex $K \in \mathcal{T}_\ell$, it satisfies*

$$(\nabla\cdot\boldsymbol{\sigma}_{\ell,\text{dis}}, q_\ell)_K = (f - \mathfrak{r}_\ell, q_\ell)_K \quad \forall K \in \mathcal{T}_\ell, \quad \forall q_\ell \in \mathbb{P}_{p_{\ell,K}(K)}. \tag{4.17}$$

Proof. Since each local contribution $\boldsymbol{\sigma}^{\mathbf{a}}_{\ell,\text{dis}}$, $\mathbf{a} \in \mathcal{V}_\ell$, lies in $\mathbf{H}(\text{div},\omega_\ell^{\mathbf{a}})$, the overall $\mathbf{H}(\text{div},\Omega)$-conformity is a direct consequence of (4.15). Next, as a result of the Neumann compatibility condition, we are allowed to take any function $q_\ell \in \mathbb{P}_{is}(\mathcal{T}_\ell^{\mathbf{a}})$ as a test function in (4.16b), without any zero mean value restriction. On each $K \in \mathcal{T}_\ell$, we have $p_{\ell,K} \le \min_{\mathbf{a}\in\mathcal{V}_K} is$. Hence, combining (4.15) with (4.16b) and employing the partition of unity $\sum_{\mathbf{a}\in\mathcal{V}_K} \psi_\ell^{\mathbf{a}}|_K = 1|_K$, we see that

$$\begin{aligned}(\nabla\cdot\boldsymbol{\sigma}_{\ell,\text{dis}}, q_\ell)_K &= \sum_{\mathbf{a}\in\mathcal{V}_K} \left(\nabla\cdot\boldsymbol{\sigma}^{\mathbf{a}}_{\ell,\text{dis}}, q_\ell\right)_K = \sum_{\mathbf{a}\in\mathcal{V}_K} (f\psi_\ell^{\mathbf{a}} - \nabla u_\ell\cdot\nabla\psi_\ell^{\mathbf{a}} - \mathfrak{r}_\ell\psi_\ell^{\mathbf{a}}, q_\ell)_K \\ &= (f - \mathfrak{r}_\ell, q_\ell)_K \quad \forall K \in \mathcal{T}_\ell \quad \forall q_\ell \in \mathbb{P}_{p_{\ell,K}}(K),\end{aligned} \tag{4.18}$$

which concludes the proof. □

4.2.3 Discrete spaces for the total residual lifting $\rho_{\ell,\text{tot}}$

Finally, for each finest vertex $\mathbf{a} \in \mathcal{V}_\ell$, we specify our choice for the $H^1_*(\omega_\ell^{\mathbf{a}})$-conforming scalar-valued spaces $V_\ell^{\mathbf{a}}$, in which we seek the local contributions of the total residual lifting $\rho_{\ell,\text{tot}}$ of Definition 3.4:

$$V_\ell^{\mathbf{a}} := \{v_\ell \in H^1(\omega_\ell^{\mathbf{a}}); v_\ell \in \mathbb{P}_{is}(K), \forall K \in \mathcal{T}_\ell^{\mathbf{a}}, (v_\ell, 1)_{\omega_\ell^{\mathbf{a}}} = 0\} \qquad \mathbf{a} \in \mathcal{V}_\ell^{\text{int}}, \tag{4.19a}$$

$$V_\ell^{\mathbf{a}} := \{v_\ell \in H^1(\omega_\ell^{\mathbf{a}}); v_\ell \in \mathbb{P}_{is}(K), \forall K \in \mathcal{T}_\ell^{\mathbf{a}}, v_\ell = 0 \text{ on } \partial\omega_\ell^{\mathbf{a}} \setminus \partial\Omega\} \quad \mathbf{a} \in \mathcal{V}_\ell^{\text{ext}}. \tag{4.19b}$$

Other choices of $V_\ell^{\mathbf{a}}$ could be also considered, in particular considering the actual polynomial degree $p_{\ell,K}$, on each simplex $K \in \mathcal{T}_\ell^{\mathbf{a}}$, instead of the local degree is would be, from a theoretical viewpoint, also sufficient.

4.3 Adaptive stopping criteria for the algebraic solver

The output of the `ESTIMATE` module enables us to assess the quality of the current approximation u_ℓ and thus make a reasonable decision if another call of the module `ONE_SOLVER_STEP` is really needed. It is considered to be unnecessary, as discussed e.g. in [13, 24, 8, 14, 19] and the references therein, if the current algebraic error is smaller than the total error by a factor $0 < \gamma_\ell < 1$ (typically of order 0.1), i.e.

$$\|\nabla\,(u_\ell^{\text{ex}} - u_\ell)\| \le \gamma_\ell \|\nabla\,(u - u_\ell)\|. \tag{4.20}$$

In order to ensure (4.20), we require that our current approximation u_ℓ satisfies the following global (safe) stopping criterion

$$\eta_{\text{alg}}(u_\ell, \mathcal{T}_\ell) \le \gamma_\ell\, \mu(u_\ell). \tag{4.21}$$

This typically allows us to avoid possible unnecessary iterations of the algebraic solver within the `ONE_SOLVER_STEP` module in case of the use of the classical stopping criterion for the algebraic solver based on the Euclidean norm of the algebraic residual vector (2.5)

$$\frac{\|\mathrm{R}_\ell\|}{\|\mathrm{F}_\ell\|} \le \varepsilon, \tag{4.22}$$

with ε prescribed at a very small value,thus without exploiting any knowledge of the error estimators.

4.4 The module `MARK`

The module `MARK` takes as input the local error estimators computed within the `ESTIMATE` module, corresponding to the current approximation u_ℓ satisfying the stopping criterion from Section 4.3. It outputs a set of marked vertices $\widetilde{\mathcal{V}}_\ell^\theta \subset \mathcal{V}_\ell$ using a bulk-chasing criterion inspired by the well-known Dörfler's marking

criterion [18]. The choice of marking vertices instead of marking simplices directly is motivated by the nature of our *hp*-decision criterion in the module `REFINE` (see Section 4.5).

For a fixed threshold parameter $\theta \in (0,1]$, the set of marked vertices $\widetilde{\mathcal{V}}_\ell^\theta$ is selected in such a way that

$$\eta\Big(u_\ell, \bigcup_{\mathbf{a}\in\widetilde{\mathcal{V}}_\ell^\theta} \mathcal{T}_\ell^{\mathbf{a}}\Big) \geq \theta\, \eta(u_\ell, \mathcal{T}_\ell), \tag{4.23}$$

where, for a subset $\mathcal{S} \subset \mathcal{T}_\ell$, we employ the notation $\eta(u_\ell, \mathcal{S}) := \{\sum_{K\in\mathcal{S}} \eta_K(u_\ell)^2\}^{1/2}$. Then, letting

$$\mathcal{M}_\ell^\theta := \bigcup_{\mathbf{a}\in\widetilde{\mathcal{V}}_\ell^\theta} \mathcal{T}_\ell^{\mathbf{a}} \subset \mathcal{T}_\ell \tag{4.24}$$

be the collection of all the simplices that belong to a patch associated with a marked vertex, we observe that (4.23) means that $\eta(u_\ell, \mathcal{M}_\ell^\theta) \geq \theta\, \eta(u_\ell, \mathcal{T}_\ell)$. To select a set $\widetilde{\mathcal{V}}_\ell^\theta$ of minimal cardinality, the mesh vertices in $\mathcal{V}_\ell$ are sorted by comparing the vertex-based error estimators $\eta(u_\ell, \mathcal{T}_\ell^{\mathbf{a}})$ for all $\mathbf{a} \in \mathcal{V}_\ell$, and a greedy algorithm is employed to build the set $\widetilde{\mathcal{V}}_\ell^\theta$. A possibly slightly larger set $\widetilde{\mathcal{V}}_\ell^\theta$ can be constructed with linear cost in terms of the number of mesh vertices by using the algorithm proposed in [18, Section 5.2].

4.5 The module `REFINE`

The module `REFINE`, as in the previous paper [15], takes as input the set of marked vertices $\widetilde{\mathcal{V}}_\ell^\theta$ and outputs the mesh $\mathcal{T}_{\ell+1}$ and the polynomial-degree distribution $\mathbf{p}_{\ell+1}$ to be used at the next step of the outer (*hp*) loop in Scheme 2. This module proceeds in three steps. First, an *hp*-decision is made on all the marked vertices, so that each marked vertex $\mathbf{a} \in \widetilde{\mathcal{V}}_\ell^\theta$ is flagged either for *h*-refinement or for *p*-refinement. This means that the set $\widetilde{\mathcal{V}}_\ell^\theta$ is split into two disjoint subsets $\widetilde{\mathcal{V}}_\ell^\theta = \widetilde{\mathcal{V}}_\ell^h \cup \widetilde{\mathcal{V}}_\ell^p$ with obvious notation. Then, in the second step, the subsets $\widetilde{\mathcal{V}}_\ell^h$ and $\widetilde{\mathcal{V}}_\ell^p$ are used to define subsets $\mathcal{M}_\ell^h$ and $\mathcal{M}_\ell^p$ of the set of marked simplices $\mathcal{M}_\ell^\theta$ (see (4.24)). The subsets $\mathcal{M}_\ell^h$ and $\mathcal{M}_\ell^p$ are not necessarily disjoint which means that some simplices can be flagged for *hp*-refinement. Finally, the two subsets $\mathcal{M}_\ell^h$ and $\mathcal{M}_\ell^p$ are used to construct $\mathcal{T}_{\ell+1}$ and $\mathbf{p}_{\ell+1}$.

4.5.1 *hp*-decision on vertices

Our *hp*-decision on marked vertices is made on the basis of two local primal solves on the patch $\mathcal{T}_\ell^{\mathbf{a}}$ attached to each marked vertex $\mathbf{a} \in \widetilde{\mathcal{V}}_\ell^\theta$. The idea is to construct two distinct local patch-based spaces in order to emulate separately the effects of *h*- and *p*-refinement. We first consider the case where the two local primal solves use Dirichlet conditions. Let us denote the polynomial-degree distribution in the patch $\mathcal{T}_\ell^{\mathbf{a}}$ by the vector $\mathbf{p}_\ell^{\mathbf{a}} := (p_{\ell,K})_{K\in\mathcal{T}_\ell^{\mathbf{a}}}$.

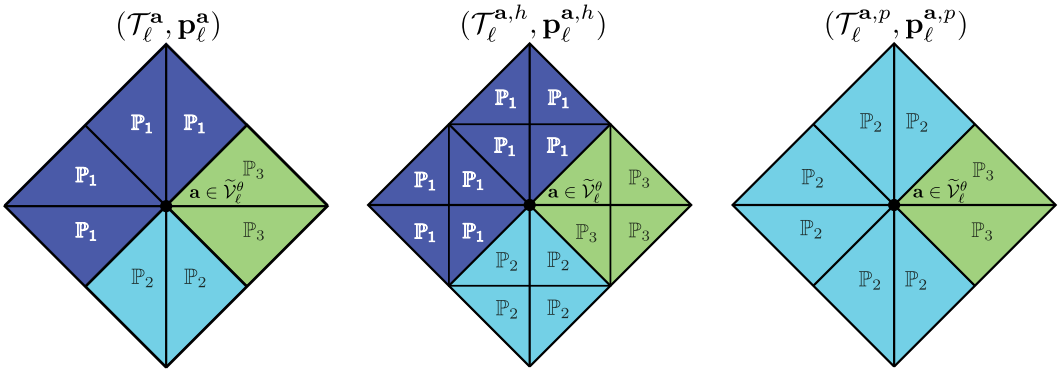

Figure 3: An example of patch $\mathcal{T}_\ell^{\mathbf{a}}$ together with its polynomial-degree distribution $\mathbf{p}_\ell^{\mathbf{a}}$ (*left*), its *h*-refined version (*center*), and its *p*-refined version (*right*) from Definitions 4.6 and 4.7, respectively.

Definition 4.6 (h-refinement residual – Dirichlet conditions)**.** *Let $\mathbf{a} \in \widetilde{\mathcal{V}}_\ell^\theta$ be a marked vertex with associated patch $\mathcal{T}_\ell^{\mathbf{a}}$ and polynomial-degree distribution $\mathbf{p}_\ell^{\mathbf{a}}$. We set*

$$V_\ell^{\mathbf{a},h} := \mathbb{P}_{\mathbf{p}_\ell^{\mathbf{a},h}}(\mathcal{T}_\ell^{\mathbf{a},h}) \cap H_0^1(\omega_\ell^{\mathbf{a}}), \tag{4.25}$$

where $\mathcal{T}_\ell^{\mathbf{a},h}$ is obtained as a matching simplicial refinement of $\mathcal{T}_\ell^{\mathbf{a}}$ by dividing each simplex $K \in \mathcal{T}_\ell^{\mathbf{a}}$ into at least two children simplices, and the polynomial-degree distribution $\mathbf{p}_\ell^{\mathbf{a},h}$ is obtained from $\mathbf{p}_\ell^{\mathbf{a}}$ by assigning to each newly-created simplex the same polynomial degree as its parent. Then, we let $r^{\mathbf{a},h} \in V_\ell^{\mathbf{a},h}$ solve

$$(\nabla r^{\mathbf{a},h}, \nabla v^{\mathbf{a},h})_{\omega_\ell^{\mathbf{a}}} = (f, v^{\mathbf{a},h})_{\omega_\ell^{\mathbf{a}}} - (\nabla u_\ell, \nabla v^{\mathbf{a},h})_{\omega_\ell^{\mathbf{a}}} \qquad \forall\, v^{\mathbf{a},h} \in V_\ell^{\mathbf{a},h}.$$

Definition 4.7 (p-refinement residual – Dirichlet conditions)**.** *Let $\mathbf{a} \in \widetilde{\mathcal{V}}_\ell^\theta$ be a marked vertex with associated patch $\mathcal{T}_\ell^{\mathbf{a}}$ and polynomial-degree distribution $\mathbf{p}_\ell^{\mathbf{a}}$. We set*

$$V_\ell^{\mathbf{a},p} := \mathbb{P}_{\mathbf{p}_\ell^{\mathbf{a},p}}(\mathcal{T}_\ell^{\mathbf{a},p}) \cap H_0^1(\omega_\ell^{\mathbf{a}}), \tag{4.26}$$

where $\mathcal{T}_\ell^{\mathbf{a},p} := \mathcal{T}_\ell^{\mathbf{a}}$, and the polynomial-degree distribution $\mathbf{p}_\ell^{\mathbf{a},p}$ is obtained from $\mathbf{p}_\ell^{\mathbf{a}}$ by assigning to each simplex $K \in \mathcal{T}_\ell^{\mathbf{a},p} = \mathcal{T}_\ell^{\mathbf{a}}$ the polynomial degree $p_{\ell,K} + \delta_K^{\mathbf{a}}$ where

$$\delta_K^{\mathbf{a}} := \begin{cases} 1 & \text{if } p_{\ell,K} = \min_{K' \in \mathcal{T}_\ell^{\mathbf{a}}} p_{\ell,K'}, \\ 0 & \text{otherwise.} \end{cases} \tag{4.27}$$

Then, we let $r^{\mathbf{a},p} \in V_\ell^{\mathbf{a},p}$ solve

$$(\nabla r^{\mathbf{a},p}, \nabla v^{\mathbf{a},p})_{\omega_\ell^{\mathbf{a}}} = (f, v^{\mathbf{a},p})_{\omega_\ell^{\mathbf{a}}} - (\nabla u_\ell, \nabla v^{\mathbf{a},p})_{\omega_\ell^{\mathbf{a}}} \qquad \forall\, v^{\mathbf{a},p} \in V_\ell^{\mathbf{a},p}.$$

The local residual liftings $r^{\mathbf{a},h}$ and $r^{\mathbf{a},p}$ from Definitions 4.6 and 4.7, respectively, are used to define the following two disjoint subsets of the set of marked vertices $\widetilde{\mathcal{V}}_\ell^\theta$:

$$\widetilde{\mathcal{V}}_\ell^h := \{\mathbf{a} \in \widetilde{\mathcal{V}}_\ell^\theta \mid \|\nabla r^{\mathbf{a},h}\|_{\omega_\ell^{\mathbf{a}}} \geq \|\nabla r^{\mathbf{a},p}\|_{\omega_\ell^{\mathbf{a}}}\}, \tag{4.28a}$$

$$\widetilde{\mathcal{V}}_\ell^p := \{\mathbf{a} \in \widetilde{\mathcal{V}}_\ell^\theta \mid \|\nabla r^{\mathbf{a},h}\|_{\omega_\ell^{\mathbf{a}}} < \|\nabla r^{\mathbf{a},p}\|_{\omega_\ell^{\mathbf{a}}}\}, \tag{4.28b}$$

in such a way that

$$\widetilde{\mathcal{V}}_\ell^\theta = \widetilde{\mathcal{V}}_\ell^h \cup \widetilde{\mathcal{V}}_\ell^p, \qquad \widetilde{\mathcal{V}}_\ell^h \cap \widetilde{\mathcal{V}}_\ell^p = \emptyset.$$

The above hp-decision criterion on vertices means that a marked vertex is flagged for h-refinement if $\|\nabla r^{\mathbf{a},h}\|_{\omega_\ell^{\mathbf{a}}}$ is larger than $\|\nabla r^{\mathbf{a},p}\|_{\omega_\ell^{\mathbf{a}}}$; otherwise, this vertex is flagged for p-refinement.

For the construction of the residuals $r^{\mathbf{a},h}$ and $r^{\mathbf{a},p}$ in Definitions 4.6 and 4.7, respectively, we considered homogeneous Dirichlet boundary conditions as in [15]. Alternatively, while keeping the local criterion (4.28) unchanged, it is possible to define the h- and p-refinement residuals by solving the local problems with homogeneous Neumann boundary conditions. We will also consider these alternative definitions in our numerical experiments.

Definition 4.8 (h-refinement residual – Neumann conditions)**.** *Let $\mathbf{a} \in \widetilde{\mathcal{V}}_\ell^\theta$ be a marked vertex. Let the simplicial submesh $\mathcal{T}_\ell^{\mathbf{a},h}$ and the corresponding polynomial degree distribution $\mathbf{p}_\ell^{\mathbf{a},h}$ be as in Definition 4.6. We recall the definition of space $H_*^1(\omega_\ell^{\mathbf{a}})$ in (3.7) and we set*

$$V_\ell^{\mathbf{a},h} := \mathbb{P}_{\mathbf{p}_\ell^{\mathbf{a},h}}(\mathcal{T}_\ell^{\mathbf{a},h}) \cap H_*^1(\omega_\ell^{\mathbf{a}}). \tag{4.29}$$

Then, we let $r^{\mathbf{a},h} \in V_\ell^{\mathbf{a},h}$ solve

$$(\nabla r^{\mathbf{a},h}, \nabla v^{\mathbf{a},h})_{\omega_\ell^{\mathbf{a}}} = (f, w_{\psi_\ell^{\mathbf{a}}}(v^{\mathbf{a},h}))_{\omega_\ell^{\mathbf{a}}} - (\nabla u_\ell, \nabla w_{\psi_\ell^{\mathbf{a}}}(v^{\mathbf{a},h}))_{\omega_\ell^{\mathbf{a}}} \qquad \forall\, v^{\mathbf{a},h} \in V_\ell^{\mathbf{a},h}, \tag{4.30}$$

where $w_{\psi_\ell^{\mathbf{a}}}(v^{\mathbf{a},h})$ stands for weighting a function $v^{\mathbf{a},h} \in V_\ell^{\mathbf{a},h}$ by the hat function $\psi_\ell^{\mathbf{a}}$ such that

$$w_{\psi_\ell^{\mathbf{a}}}(v^{\mathbf{a},h}) \in \mathbb{P}_{\mathbf{p}_\ell^{\mathbf{a},h}}(\mathcal{T}_\ell^{\mathbf{a},h}) \cap H^1(\omega_\ell^{\mathbf{a}}) \qquad \text{and} \qquad w_{\psi_\ell^{\mathbf{a}}}(v^{\mathbf{a},h})(\mathbf{x}) = \psi_\ell^{\mathbf{a}}(\mathbf{x}) \cdot v^{\mathbf{a},h}(\mathbf{x}) \tag{4.31}$$

with the nodes $\mathbf{x}$ uniquely determining a function in $\mathbb{P}_{\mathbf{p}_\ell^{\mathbf{a},h}}(\mathcal{T}_\ell^{\mathbf{a},h}) \cap H^1(\omega_\ell^{\mathbf{a}})$.

Definition 4.9 (p-refinement residual – Neumann conditions)**.** *Let $\mathbf{a} \in \widetilde{\mathcal{V}}_\ell^\theta$ be a marked vertex associated with the simplicial mesh $\mathcal{T}_\ell^{\mathbf{a},p}$ and corresponding polynomial degree distribution $\mathbf{p}_\ell^{\mathbf{a},p}$ as in Definition 4.7. We set*

$$V_\ell^{\mathbf{a},p} := \mathbb{P}_{\mathbf{p}_\ell^{\mathbf{a},p}}(\mathcal{T}_\ell^{\mathbf{a},p}) \cap H^1_*(\omega_\ell^{\mathbf{a}}). \tag{4.32}$$

Then, we let $r^{\mathbf{a},p} \in V_\ell^{\mathbf{a},p}$ solve

$$(\nabla r^{\mathbf{a},p}, \nabla v^{\mathbf{a},p})_{\omega_\ell^{\mathbf{a}}} = (f, w_{\psi_\ell^{\mathbf{a}}}(v^{\mathbf{a},p}))_{\omega_\ell^{\mathbf{a}}} - (\nabla u_\ell, \nabla w_{\psi_\ell^{\mathbf{a}}}(v^{\mathbf{a},p}))_{\omega_\ell^{\mathbf{a}}} \qquad \forall\, v^{\mathbf{a},p} \in V_\ell^{\mathbf{a},p}, \tag{4.33}$$

where $w_{\psi_\ell^{\mathbf{a}}}(v^{\mathbf{a},h})$, similarly to (4.31), stands for weighting a function $v^{\mathbf{a},p} \in V_\ell^{\mathbf{a},p}$ by a hat function $\psi_\ell^{\mathbf{a}}$ such that

$$w_{\psi_\ell^{\mathbf{a}}}(v^{\mathbf{a},p}) \in \mathbb{P}_{\mathbf{p}_\ell^{\mathbf{a},p}}(\mathcal{T}_\ell^{\mathbf{a},p}) \cap H^1(\omega_\ell^{\mathbf{a}}) \qquad \text{and} \qquad w_{\psi_\ell^{\mathbf{a}}}(v^{\mathbf{a},p})(\mathbf{x}) = \psi_\ell^{\mathbf{a}}(\mathbf{x}) \cdot v^{\mathbf{a},p}(\mathbf{x})$$

with the nodes $\mathbf{x}$ uniquely determining a function in $\mathbb{P}_{\mathbf{p}_\ell^{\mathbf{a},p}}(\mathcal{T}_\ell^{\mathbf{a},p}) \cap H^1(\omega_\ell^{\mathbf{a}})$.

4.5.2 *hp*-decision on simplices

The second step in the module `REFINE` is to use the subsets $\widetilde{\mathcal{V}}_\ell^h$ and $\widetilde{\mathcal{V}}_\ell^p$ to decide whether h-, p- , or hp-refinement should be performed on each simplex having at least one flagged vertex. To this purpose, we define the following subsets:

$$\mathcal{M}_\ell^h := \{K \in \mathcal{T}_\ell \mid \mathcal{V}_K \cap \widetilde{\mathcal{V}}_\ell^h \neq \emptyset\} \subset \mathcal{M}_\ell^\theta, \tag{4.34a}$$

$$\mathcal{M}_\ell^p := \{K \in \mathcal{T}_\ell \mid \mathcal{V}_K \cap \widetilde{\mathcal{V}}_\ell^p \neq \emptyset\} \subset \mathcal{M}_\ell^\theta. \tag{4.34b}$$

In other words, a simplex $K \in \mathcal{T}_\ell$ is flagged for h-refinement (resp., p-refinement) if it has at least one vertex flagged for h-refinement (resp., p-refinement). Note that the subsets $\mathcal{M}_\ell^h$ and $\mathcal{M}_\ell^p$ are not necessarily disjoint since a simplex can have some vertices flagged for h-refinement and others flagged for p-refinement; such simplices are then flagged for hp-refinement. Note also that $\mathcal{M}_\ell^h \cup \mathcal{M}_\ell^p = \cup_{\mathbf{a} \in \widetilde{\mathcal{V}}_\ell^\theta} \mathcal{T}_\ell^{\mathbf{a}} = \mathcal{M}_\ell^\theta$ is indeed the set of marked simplices considered in the module `MARK`.

4.5.3 *hp*-refinement

In this last and final step, the subsets $\mathcal{M}_\ell^h$ and $\mathcal{M}_\ell^p$ are used to produce first the next mesh $\mathcal{T}_{\ell+1}$ and then the next polynomial-degree distribution $\mathbf{p}_{\ell+1}$ on the mesh $\mathcal{T}_{\ell+1}$.

The next mesh $\mathcal{T}_{\ell+1}$ is a matching simplicial refinement of $\mathcal{T}_\ell$ obtained by dividing each flagged simplex $K \in \mathcal{M}_\ell^h$ into at least two simplices in a way that is consistent with the matching simplicial refinement of $\mathcal{T}_\ell^{\mathbf{a}}$ considered in Definition 4.6 to build $\mathcal{T}_\ell^{\mathbf{a},h}$, i.e., such that $\mathcal{T}_\ell^{\mathbf{a},h} \subset \mathcal{T}_{\ell+1}$ for all $\mathbf{a} \in \widetilde{\mathcal{V}}_\ell^h$. Note that to preserve the conformity of the mesh, additional refinements beyond the set of flagged simplices $\mathcal{M}_\ell^h$ may be carried out when building $\mathcal{T}_{\ell+1}$. Several algorithms can be considered to refine the mesh. In our numerical experiments, we used the newest vertex bisection algorithm [30, 31].

After having constructed the next mesh $\mathcal{T}_{\ell+1}$, we assign the next polynomial-degree distribution $\mathbf{p}_{\ell+1}$ as follows. For all $K \in \mathcal{T}_{\ell+1}$, let $\widetilde{K}$ denote its parent simplex in $\mathcal{T}_\ell$. We then set

$$p_{\ell+1,K} := p_{\ell,\widetilde{K}} \qquad \text{if } \widetilde{K} \notin \mathcal{M}_\ell^p, \tag{4.35}$$

that is, we assign the same polynomial degree to the children of a simplex that is not flagged for p-refinement, whereas we set

$$p_{\ell+1,K} := \max_{\mathbf{a} \in \mathcal{V}_{\widetilde{K}} \cap \widetilde{\mathcal{V}}_\ell^p} \left(p_{\ell,\widetilde{K}} + \delta_{\widetilde{K}}^{\mathbf{a}}\right) \qquad \text{if } \widetilde{K} \in \mathcal{M}_\ell^p, \tag{4.36}$$

that is, we assign to the children of a simplex $\widetilde{K} \in \mathcal{M}_\ell^p$ flagged for p-refinement the largest of the polynomial degrees considered in Definition 4.7 to build the local residual liftings associated with the vertices of $\widetilde{K}$ flagged for p-refinement.

5 Guaranteed bound on the error reduction

In this section we extend the results of our previous work [15, Section 5], where a computable guaranteed bound on the error reduction factor between two consecutive steps of an *hp*-adaptive procedure with an exact solver has been derived. We recall that the adaptive strategy of [15] generates a sequence of exact finite element solutions $\{u_\ell^{\mathrm{ex}}\}_{\ell\geq 0}$. For a fixed $\ell \geq 0$, let us denote by $C_{\mathrm{red}}^{\mathrm{ex}}$ the bound on the energy error reduction factor between $u_\ell^{\mathrm{ex}} \in V_\ell$ and $u_{\ell+1}^{\mathrm{ex}} \in V_{\ell+1}$ derived in [15, Theorem 5.2] such that

$$\|\nabla(u - u_{\ell+1}^{\mathrm{ex}})\| \leq C_{\mathrm{red}}^{\mathrm{ex}} \|\nabla(u - u_\ell^{\mathrm{ex}})\| \quad \text{with} \quad 0 \leq C_{\mathrm{red}}^{\mathrm{ex}} \leq 1. \tag{5.1}$$

Using the current notation, and letting $\omega_\ell := \cup_{\mathbf{a}\in\widetilde{\mathcal{V}}_\ell^\theta} \omega_\ell^{\mathbf{a}}$, the definition of $C_{\mathrm{red}}^{\mathrm{ex}}$ reads

$$C_{\mathrm{red}}^{\mathrm{ex}} := \sqrt{1 - \left(\theta \frac{\underline{\eta}_{\mathcal{M}_\ell^\theta}^{\mathrm{ex}}}{\eta(u_\ell^{\mathrm{ex}}, \mathcal{M}_\ell)}\right)^2}, \tag{5.2}$$

with the total error estimator $\eta(u_\ell^{\mathrm{ex}}, \mathcal{M}_\ell)$ of Theorem 3.3 (the local algebraic error estimator $\eta_{\mathrm{alg},K}(u_\ell^{\mathrm{ex}}) := 0$ for each $K \in \mathcal{T}_\ell$), and the discrete lower bound $\underline{\eta}_{\mathcal{M}_\ell^\theta}^{\mathrm{ex}} \leq \|\nabla(u_{\ell+1}^{\mathrm{ex}} - u_\ell^{\mathrm{ex}})\|_{\omega_\ell}$ defined in [15, Lemma 5.1].

The aim of this section is to derive an equivalent of the bound (5.1) between the two *inexact* solutions $u_\ell \in V_\ell$ and $u_{\ell+1} \in V_{\ell+1}$ obtained by the iterative procedure of Scheme 2 in the form

$$\|\nabla(u - u_{\ell+1})\| \leq C_{\mathrm{red}} \|\nabla(u - u_\ell)\|.$$

It turns out essential to first estimate a guaranteed bound on the error reduction between the current inexact solution $u_\ell \in V_\ell$ and the (unavailable) exact solution on the next level $u_{\ell+1}^{\mathrm{ex}} \in V_{\ell+1}$. For this we start by extending the discrete lower bound of [15, Lemma 5.1] to the present setting:

Lemma 5.1 (Guaranteed lower bound on the incremental error on marked simplices)**.** *Let the mesh $\mathcal{T}_{\ell+1}$ and the polynomial-degree distribution $\mathbf{p}_{\ell+1}$ result from the* `REFINE` *module of Section 4.5, and recall that $V_{\ell+1} = \mathbb{P}_{\mathbf{p}_{\ell+1}}(\mathcal{T}_{\ell+1}) \cap H_0^1(\Omega)$ is the finite element space to be used on step $(\ell+1)$ of the outer (hp) loop of Scheme 2. For all the marked vertices $\mathbf{a} \in \widetilde{\mathcal{V}}_\ell^\theta$, let us set, in extension of (4.25), (4.26),*

$$V_\ell^{\mathbf{a},hp} := V_{\ell+1}|_{\omega_\ell^{\mathbf{a}}} \cap H_0^1(\omega_\ell^{\mathbf{a}}), \tag{5.3}$$

and construct the residual lifting $r^{\mathbf{a},hp} \in V_\ell^{\mathbf{a},hp}$ by solving

$$(\nabla r^{\mathbf{a},hp}, \nabla v^{\mathbf{a},hp})_{\omega_\ell^{\mathbf{a}}} = (f, v^{\mathbf{a},hp})_{\omega_\ell^{\mathbf{a}}} - (\nabla u_\ell, \nabla v^{\mathbf{a},hp})_{\omega_\ell^{\mathbf{a}}} \qquad \forall\, v^{\mathbf{a},hp} \in V_\ell^{\mathbf{a},hp}. \tag{5.4}$$

Then, after extending $r^{\mathbf{a},hp}$ by zero outside $\omega_\ell^{\mathbf{a}}$, for the current inexact approximation $u_\ell \in V_\ell$ and the exact approximation $u_{\ell+1}^{\mathrm{ex}} \in V_{\ell+1}$ on the next level, the following holds true:

$$\|\nabla(u_{\ell+1}^{\mathrm{ex}} - u_\ell)\|_{\omega_\ell} \geq \underline{\eta}_{\mathcal{M}_\ell^\theta}, \quad \underline{\eta}_{\mathcal{M}_\ell^\theta} := \begin{cases} \dfrac{\sum_{\mathbf{a}\in\widetilde{\mathcal{V}}_\ell^\theta} \left\|\nabla r^{\mathbf{a},hp}\right\|_{\omega_\ell^{\mathbf{a}}}^2}{\left\|\nabla\left(\sum_{\mathbf{a}\in\widetilde{\mathcal{V}}_\ell^\theta} r^{\mathbf{a},hp}\right)\right\|_{\omega_\ell}} & \text{if } \sum_{\mathbf{a}\in\widetilde{\mathcal{V}}_\ell^\theta} r^{\mathbf{a},hp} \neq 0, \\ 0 & \text{otherwise.} \end{cases} \tag{5.5}$$

Proof. We remark that the definition of the residual liftings $r^{\mathbf{a},hp}$ (5.4) employs directly the inexact approximation u_ℓ unlike in [15, Lemma 5.1] where u_ℓ^{ex} (in the present notation) was considered. Nevertheless, the arguments to prove the lower bound $\underline{\eta}_{\mathcal{M}_\ell^\theta}^{\mathrm{ex}}$ of [15, Lemma 5.1] stay valid and can be used to show (5.5). □

In case of the use of residuals $r^{\mathbf{a},h}$ and $r^{\mathbf{a},p}$ from Definitions 4.8 and 4.9, respectively, in the local criterion (4.28) within the `REFINE` module, the above lower bound can be adjusted as well.

Lemma 5.2 (Guaranteed lower bound on the incremental error on marked simplices – alternative definition)**.** *Let the assumptions of Lemma 5.1 be satisfied. Moreover, let us set for all the marked vertices $\mathbf{a} \in \widetilde{\mathcal{V}}_\ell^\theta$, in extension of (4.29) and (4.32),*

$$V_\ell^{\mathbf{a},hp} := V_{\ell+1}|_{\omega_\ell^{\mathbf{a}}} \cap H_*^1(\omega_\ell^{\mathbf{a}}). \tag{5.6}$$

Then, for each marked vertex $\mathbf{a} \in \widetilde{\mathcal{V}}_\ell^\theta$*, construct the residual lifting* $r^{\mathbf{a},hp} \in V_\ell^{\mathbf{a},hp}$ *by solving*

$$(\nabla r^{\mathbf{a},hp}, \nabla v^{\mathbf{a},hp})_{\omega_\ell^{\mathbf{a}}} = (f, w_{\psi_\ell^{\mathbf{a}}}(v^{\mathbf{a},hp}))_{\omega_\ell^{\mathbf{a}}} - (\nabla u_\ell, \nabla w_{\psi_\ell^{\mathbf{a}}}(v^{\mathbf{a},hp}))_{\omega_\ell^{\mathbf{a}}} \quad \forall\, v^{\mathbf{a},hp} \in V_\ell^{\mathbf{a},hp}, \tag{5.7}$$

where $w_{\psi_\ell^{\mathbf{a}}}(v^{\mathbf{a},hp})$ *stands for weighting a function* $v^{\mathbf{a},hp} \in V_\ell^{\mathbf{a},hp}$ *by hat function* $\psi_\ell^{\mathbf{a}}$ *such that*

$$w_{\psi_\ell^{\mathbf{a}}}(v^{\mathbf{a},p}) \in V_{\ell+1}|_{\omega_\ell^{\mathbf{a}}} \qquad \text{and} \qquad w_{\psi_\ell^{\mathbf{a}}}(v^{\mathbf{a},p})(\mathbf{x}) = \psi_\ell^{\mathbf{a}}(\mathbf{x}) \cdot v^{\mathbf{a},p}(\mathbf{x})$$

with the nodes $\mathbf{x}$ *uniquely determining a function in* $V_{\ell+1}|_{\omega_\ell^{\mathbf{a}}}$*. After extending each* $r^{\mathbf{a},hp}$ *by zero outside* $\omega_\ell^{\mathbf{a}}$*, the following lower bound holds true:*

$$\|\nabla(u_{\ell+1}^{\mathrm{ex}} - u_\ell)\|_{\omega_\ell} \geq \underline{\eta}_{\mathcal{M}_\ell^\theta}, \quad \underline{\eta}_{\mathcal{M}_\ell^\theta} := \begin{cases} \dfrac{\sum_{\mathbf{a}\in\widetilde{\mathcal{V}}_\ell^\theta} \|\nabla r^{\mathbf{a},hp}\|_{\omega_\ell^{\mathbf{a}}}^2}{\left\|\nabla\left(\sum_{\mathbf{a}\in\widetilde{\mathcal{V}}_\ell^\theta} w_{\psi_\ell^{\mathbf{a}}}(r^{\mathbf{a},hp})\right)\right\|_{\omega_\ell}} & \text{if } \sum_{\mathbf{a}\in\widetilde{\mathcal{V}}_\ell^\theta} r^{\mathbf{a},hp} \neq 0, \\ 0 & \text{otherwise.} \end{cases} \tag{5.8}$$

Proof. Let us note that $(u_{\ell+1}^{\mathrm{ex}} - u_\ell)|_{\omega_\ell}$ belongs to the space $V_{\ell+1}(\omega_\ell)$, a restriction of the finite element space $V_{\ell+1}$ to ω_ℓ. However, note that it does not necessarily belong to the homogeneous Dirichlet subspace $V_{\ell+1}^0(\omega_\ell)$. The definition of the energy norm $\|\nabla(u_{\ell+1}^{\mathrm{ex}} - u_\ell)\|_{\omega_\ell}$ and the fact that $v_{\ell+1} \in V_{\ell+1}^0(\omega_\ell)$ extended by zero outside ω_ℓ is a member of the space $V_{\ell+1}$ so that it can be used as a test function in the definition (2.3) of $u_{\ell+1}^{\mathrm{ex}}$ on the mesh $\mathcal{T}_{\ell+1}$ yield

$$\begin{aligned} \|\nabla(u_{\ell+1}^{\mathrm{ex}} - u_\ell)\|_{\omega_\ell} &= \sup_{v_{\ell+1}\in V_{\ell+1}(\omega_\ell)} \frac{(\nabla(u_{\ell+1}^{\mathrm{ex}} - u_\ell), \nabla v_{\ell+1})_{\omega_\ell}}{\|\nabla v_{\ell+1}\|_{\omega_\ell}} \\ &\geq \sup_{v_{\ell+1}\in V_{\ell+1}^0(\omega_\ell)} \frac{(\nabla(u_{\ell+1}^{\mathrm{ex}} - u_\ell), \nabla v_{\ell+1})_{\omega_\ell}}{\|\nabla v_{\ell+1}\|_{\omega_\ell}} \\ &= \sup_{v_{\ell+1}\in V_{\ell+1}^0(\omega_\ell)} \frac{(f, v_{\ell+1})_{\omega_\ell} - (\nabla u_\ell, \nabla v_{\ell+1})_{\omega_\ell}}{\|\nabla v_{\ell+1}\|_{\omega_\ell}}. \end{aligned}$$

Now, choose the test function $v_{\ell+1} := \sum_{\mathbf{a}\in\widetilde{\mathcal{V}}_\ell^\theta} w_{\psi_\ell^{\mathbf{a}}}(r^{\mathbf{a},hp})$; note that, due to the weighting $w_{\psi_\ell^{\mathbf{a}}}(\cdot)$, such choice of $v_{\ell+1}$ indeed belongs to $V_{\ell+1}^0(\omega_\ell)$. Then, we infer that

$$\begin{aligned} &\left(f, \sum_{\mathbf{a}\in\widetilde{\mathcal{V}}_\ell^\theta} w_{\psi_\ell^{\mathbf{a}}}(r^{\mathbf{a},hp})\right)_{\omega_\ell} - \left(\nabla u_\ell, \sum_{\mathbf{a}\in\widetilde{\mathcal{V}}_\ell^\theta} w_{\psi_\ell^{\mathbf{a}}}(r^{\mathbf{a},hp})\right)_{\omega_\ell} \\ &\qquad = \sum_{\mathbf{a}\in\widetilde{\mathcal{V}}_\ell^\theta} \{(f, w_{\psi_\ell^{\mathbf{a}}}(r^{\mathbf{a},hp}))_{\omega_\ell} - (\nabla u_\ell, \nabla w_{\psi_\ell^{\mathbf{a}}}(r^{\mathbf{a},hp}))_{\omega_\ell}\} = \sum_{\mathbf{a}\in\widetilde{\mathcal{V}}_\ell^\theta} \|\nabla r^{\mathbf{a},hp}\|_{\omega_\ell^{\mathbf{a}}}^2, \end{aligned}$$

where we employed (5.7) with $r^{\mathbf{a},hp}$ as a test function. This implies the assertion (5.8). □

We now proceed with an intermediate result giving a guaranteed bound on the error reduction factor between the current inexact approximation u_ℓ and the (unavailable) next level exact solution $u_{\ell+1}^{\mathrm{ex}}$.

Lemma 5.3 (Auxiliary guaranteed bound on the energy error reduction factor)**.** *Let* θ *be the threshold parameter used within the module* `MARK` *of Section 4.4 and let the mesh* $\mathcal{T}_{\ell+1}$ *and the polynomial degree distribution* $\mathbf{p}_{\ell+1}$ *be given by the* `REFINE` *module of Section 4.5. Next, let* $V_{\ell+1} := \mathbb{P}_{\mathbf{p}_{\ell+1}}(\mathcal{T}_{\ell+1}) \cap H_0^1(\Omega)$ *be the space to be used on step* $(\ell+1)$ *of the inexact hp-adaptive algorithm described in Scheme 2. Let* $\underline{\eta}_{\mathcal{M}_\ell^\theta}$ *be the lower bound defined by (5.5) or (5.8), depending on the choice of the construction of residuals* $r^{\mathbf{a},h}$*,* $r^{\mathbf{a},p}$ *used within the* `REFINE` *module. Then, unless* $\eta(u_\ell, \mathcal{T}_\ell) = 0$*, in which case* $u_\ell = u$*, and the outer (hp) loop terminates, the exact finite element solution* $u_{\ell+1}^{\mathrm{ex}} \in V_{\ell+1}$ *satisfies*

$$\|\nabla(u - u_{\ell+1}^{\mathrm{ex}})\| \leq C_{\mathrm{red}}^* \|\nabla(u - u_\ell)\| \quad \text{with} \quad 0 \leq C_{\mathrm{red}}^* := \sqrt{1 - \frac{\underline{\eta}_{\mathcal{M}_\ell^\theta}^2}{\eta^2(u_\ell, \mathcal{T}_\ell)}} \leq 1. \tag{5.9}$$

Proof. Since the Galerkin orthogonality property between the current approximation $u_\ell \in V_\ell$ and the exact finite element solution $u_{\ell+1}^{\mathrm{ex}} \in V_{\ell+1}$ holds true, we have

$$\|\nabla(u - u_{\ell+1}^{\mathrm{ex}})\|^2 = \|\nabla(u - u_\ell)\|^2 - \|\nabla(u_{\ell+1}^{\mathrm{ex}} - u_\ell)\|^2. \tag{5.10}$$

Afterwards, employing the lower bound $\underline{\eta}_{\mathcal{M}_\ell^\theta}$ and the total error upper bound $\eta(u_\ell, \mathcal{T}_\ell)$ from (3.5) in (5.10) yields

$$\|\nabla(u - u_{\ell+1}^{\mathrm{ex}})\|^2 \leq \|\nabla(u - u_\ell)\|^2 - \underline{\eta}_{\mathcal{M}_\ell^\theta}^2 \frac{\|\nabla(u - u_\ell)\|^2}{\|\nabla(u - u_\ell)\|^2} \leq \|\nabla(u - u_\ell)\|^2 \left(1 - \frac{\underline{\eta}_{\mathcal{M}_\ell^\theta}^2}{\eta^2(u_\ell, \mathcal{T}_\ell)}\right).$$

The assertion (5.9) then follows by taking the square root. We note that (5.10) implies $\|\nabla(u_{\ell+1}^{\mathrm{ex}} - u_\ell)\| \leq \|\nabla(u - u_\ell)\|$. Then, the total error upper bound (3.5) and lower bound $\underline{\eta}_{\mathcal{M}_\ell^\theta}$ from (5.5) or (5.8) yield $\underline{\eta}_{\mathcal{M}_\ell^\theta} \leq \eta(u_\ell, \mathcal{T}_\ell)$. So the square root of $\left(1 - \frac{\underline{\eta}_{\mathcal{M}_\ell^\theta}^2}{\eta^2(u_\ell, \mathcal{T}_\ell)}\right)$ always exists. □

Finally, we are ready to present the result on a computable guaranteed bound on the reduction factor in the inexact setting:

Theorem 5.4 (Guaranteed bound on the energy error reduction factor between two inexact solutions)**.** *Let the assumptions of Lemma 5.3 be satisfied and let C_{red}^* be given by (5.9). Moreover, let $u_{\ell+1} \in V_{\ell+1}$ be the inexact finite element approximation on step $(\ell+1)$ of the inexact hp-adaptive algorithm described in Scheme 2, satisfying the global stopping criterion*

$$\eta_{\mathrm{alg}}(u_{\ell+1}, \mathcal{T}_{\ell+1}) \leq \gamma_{\ell+1}\, \mu(u_{\ell+1}), \tag{5.11}$$

with the parameter

$$0 \leq \gamma_{\ell+1} \leq (1 - C_{\mathrm{red}}^*). \tag{5.12}$$

Then, the resulting error reduction between the inexact solution $u_\ell \in V_\ell$ from the current step ℓ and the next approximation $u_{\ell+1}$ to be computed on the next step verifies

$$\|\nabla(u - u_{\ell+1})\| \leq C_{\mathrm{red}} \|\nabla(u - u_\ell)\| \qquad \text{with} \qquad 0 \leq C_{\mathrm{red}} := \frac{C_{\mathrm{red}}^*}{(1 - \gamma_{\ell+1})} \leq 1. \tag{5.13}$$

Proof. We start by adding and subtracting $\nabla u_{\ell+1}^{\mathrm{ex}}$ inside the norm on the left hand side of (5.13). The triangle inequality then yields

$$\|\nabla(u - u_{\ell+1})\| \leq \|\nabla(u - u_{\ell+1}^{\mathrm{ex}})\| + \|\nabla(u_{\ell+1}^{\mathrm{ex}} - u_{\ell+1})\|. \tag{5.14}$$

For bounding the first term, we employ the auxiliary bound (5.9). The second term of (5.14), the algebraic error on step $(\ell+1)$, is first bounded from above by the algebraic error estimate (3.6). Then, the stopping criterion (5.11) with the parameter $\gamma_{\ell+1}$ in combination with the total energy error lower bound (3.9) give

$$\|\nabla(u_{\ell+1}^{\mathrm{ex}} - u_{\ell+1})\| \leq \eta_{\mathrm{alg}}(u_{\ell+1}, \mathcal{T}_{\ell+1}) \leq \gamma_{\ell+1}\, \mu(u_{\ell+1}) \leq \gamma_{\ell+1}\, \|\nabla(u - u_{\ell+1})\|,$$

whence we infer (5.13). The condition (5.12) on parameter $\gamma_{\ell+1}$ then ensures the upper bound $C_{\mathrm{red}} \leq 1$. □

Remark 5.5 (Extreme case equivalent to the use of an exact solver)**.** *In Theorem 5.4 we do not exclude the extreme case where the auxiliary upper bound $C_{\mathrm{red}}^* = 1$. This in turn leads to the stopping criterion (5.11) with the parameter $\gamma_{\ell+1} = 0$, which is equivalent to computing the exact finite element solution $u_{\ell+1}^{\mathrm{ex}}$. However, we note that in our numerical experiments, reported in Section 6, we never encountered such a situation where the exact solver would be necessary.*

Remark 5.6 (Motivation)**.** *We believe that, under some additional assumptions on the refinements, such as the the interior node property [32], one could actually show $C_{\mathrm{red}}^* < 1$. The convergence of the proposed method would then easily follow. We do not further address this topic here.*

6 Numerical experiments

We now illustrate the capabilities and robustness of the proposed inexact *hp*-adaptive algorithm on two-dimensional test cases. We consider two problems with a (relatively) smooth weak solution and one with a singular weak solution.

We focus on the influence of the inexact algebraic solver on the performance of the proposed *hp*-refinement strategy described in Section 4.5. While employing the adaptive stopping criterion (4.21) with the parameter γ_ℓ satisfying (5.12), we assess the quality of the guaranteed bound on the reduction factor C_{red} from Theorem 5.4 throughout the inexact *hp*-adaptive algorithm in terms of the effectivity index defined as

$$I_{\mathrm{red}}^{\mathrm{eff}} := \frac{C_{\mathrm{red}}}{\frac{\|\nabla(u-u_{\ell+1})\|}{\|\nabla(u-u_\ell)\|}}. \tag{6.1}$$

We also verify the sharpness of the underlying discrete lower bound $\underline{\eta}_{\mathcal{M}_\ell^\theta}$ given by (5.5) or (5.8) in terms of the effectivity index defined as

$$I_{\mathrm{LB}}^{\mathrm{eff}} := \frac{\|\nabla(u_{\ell+1}^{\mathrm{ex}} - u_\ell)\|_{\omega_\ell}}{\underline{\eta}_{\mathcal{M}_\ell^\theta}}. \tag{6.2}$$

Besides that, we are interested in the comparison of the different stopping criteria for the algebraic solver with regard to the number of necessary inner (algebraic) iterations per step of the outer (*hp*) loop, the time spent on algebraic computations and their influence on the overall inexact *hp*-adaptive algorithm. In all the example problems, we use the *hp*-multigrid method with 5 pre-smoothing Gauss–Seidel steps and no post-smoothing as the algebraic solver. We always take into account at most 10 last levels available from the current hierarchy of adaptively refined meshes at our disposal for the *hp*-multigrid solver, as well as for the algebraic error flux reconstruction $\boldsymbol{\sigma}_{\ell,\mathrm{alg}}$ from Definition 4.1. In other words, if the outer (*hp*) loop step $\ell \geq 10$, we adjust the range of the sum (4.4) in the following way

$$\boldsymbol{\sigma}_{\ell,\mathrm{alg}} := \sum_{j=\ell-8}^{\ell} \sum_{\mathbf{a}\in\mathcal{V}_{j-1}} \boldsymbol{\sigma}_{j,\mathrm{alg}}^{\mathbf{a}},$$

thus we solve problem (4.5) on level $j = \ell - 8$ and problem (4.7) on levels $\ell - 7 \leq j \leq \ell$. Similarly, the multigrid solver uses the hierarchy $\{\mathcal{T}_j, \mathbf{p}_j\}_{\ell-9\leq j\leq \ell}$, for $\ell \geq 10$, instead of the complete available hierarchy $\{\mathcal{T}_j, \mathbf{p}_j\}_{0\leq j\leq \ell}$, which is used in case of the outer (*hp*) loop step ℓ being lower than 10. The (well-established, see e.g. [33, page 65]) choice $\theta = 0.5$ for the marking parameter in (4.23) is considered. We examine the proposed adaptive *hp*-refinement strategy employing the local residuals $r^{\mathbf{a},h}$ and $r^{\mathbf{a},p}$ defined via solving the local problems with either homogeneous Dirichlet (Definitions 4.6 and 4.7) or homogeneous Neumann boundary conditions (Definitions 4.8 and 4.9). As mentioned above, we employ the newest vertex bisection algorithm [30] to perform *h*-refinement and we use the polynomial-degree increment (4.27) to perform *p*-refinement. Dunavant quadratures are employed on the reference unit simplex to compute exactly all the integrals involving polynomial functions; in particular, this means that the computation of the estimators is free of quadrature errors.

6.1 Smooth solution (sharp Gaussian)

As the first test case, we consider the model problem (1.1) posed on a square domain $\Omega := (-1,1)\times(-1,1)$ with a weak solution containing a rather sharp peak

$$u(x,y) = (x^2-1)(y^2-1)\exp\left(-100(x^2+y^2)\right).$$

We start the computation with a coarse criss-cross mesh $\mathcal{T}_0$ with $\max_{K\in\mathcal{T}_0} h_K = 0.25$ and a uniform polynomial-degree distribution equal to 1 on all triangles. In the following, we present the results obtained using the proposed *hp*-refinement strategy employing the local residuals $r^{\mathbf{a},h}$ and $r^{\mathbf{a},p}$ defined by either the local Dirichlet or local Neumann problems.

6.1.1 Strategy driven by the local Dirichlet problems

Firstly, in Figure 4 we investigate the accuracy of the predicted reduction factor $C_{\rm red}$ (left panel) and the lower bound $\underline{\eta}_{\mathcal{M}_\ell^\theta}$ (center panel) by means of their effectivity indices (6.1) and (6.2) throughout the inexact *hp*-adaptive algorithm described in Scheme 2 with the module `REFINE` driven by solving the local Dirichlet problems from Definitions 4.6 and 4.7. We find the effectivity indices in both cases close to the optimal value of one. In all our numerical experiments, we use $\gamma_{\ell+1} = 0.1$ as the default value of the parameter $\gamma_{\ell+1}$ employed in the stopping criterion (5.11). However, at some steps of the outer (*hp*) loop, we are forced to lower its value in order to ensure the condition (5.12), so that the actual value of the stopping criterion parameter (reported in the right panel of Figure 4) to be used at the next outer (*hp*) loop step is determined as $\gamma_{\ell+1} = \min\{0.1, \alpha(1 - C^*_{\rm red})\}$, with $\alpha = 0.95$ in our implementation.

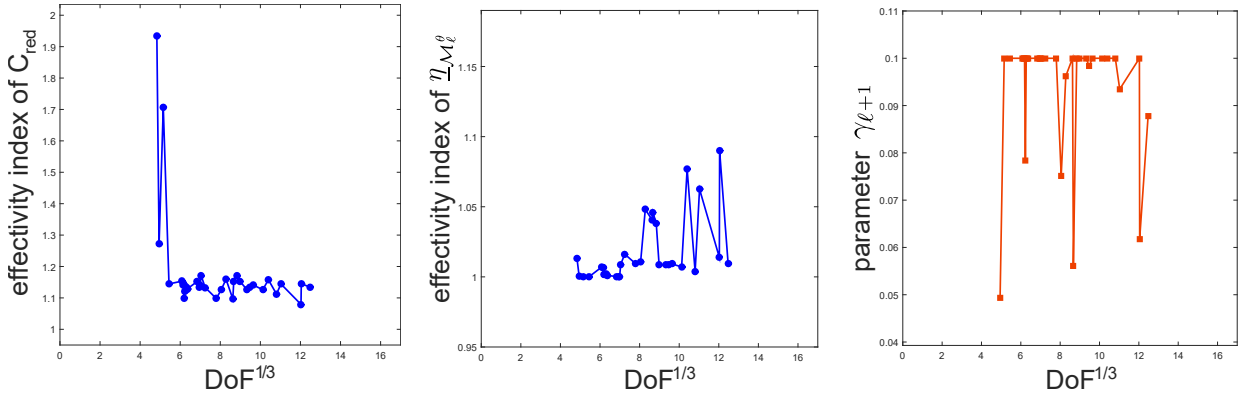

Figure 4: [Sharp-Gaussian of Section 6.1] Effectivity index for the error reduction factor estimate $C_{\rm red}$ of Theorem 5.4 given by (6.1) (*left*); Effectivity index for the discrete lower bound $\underline{\eta}_{\mathcal{M}_\ell^\theta}$ of Lemma 5.1 given by (6.2) (*center*); corresponding values of the parameter $\gamma_{\ell+1}$ used in (5.13) (*right*).

A quantitative assessment of various stopping criteria for the inexact solver is presented in Figure 5 (left panel) where we plot the relative error $\|\nabla(u - u_\ell)\|/\|\nabla u\|$ as a function of the cumulative time spent on the algebraic computations in linear-logarithmic scale (not including the time to compute the estimators). We observe that the strategy with inexact solver piloted by the present adaptive stopping criterion leads to the steepest error decrease with respect to the computational effort. This is mostly due to cutting off unnecessary algebraic iterations as reported in the right panel of Figure 5. Figure 6 (left panel) displays

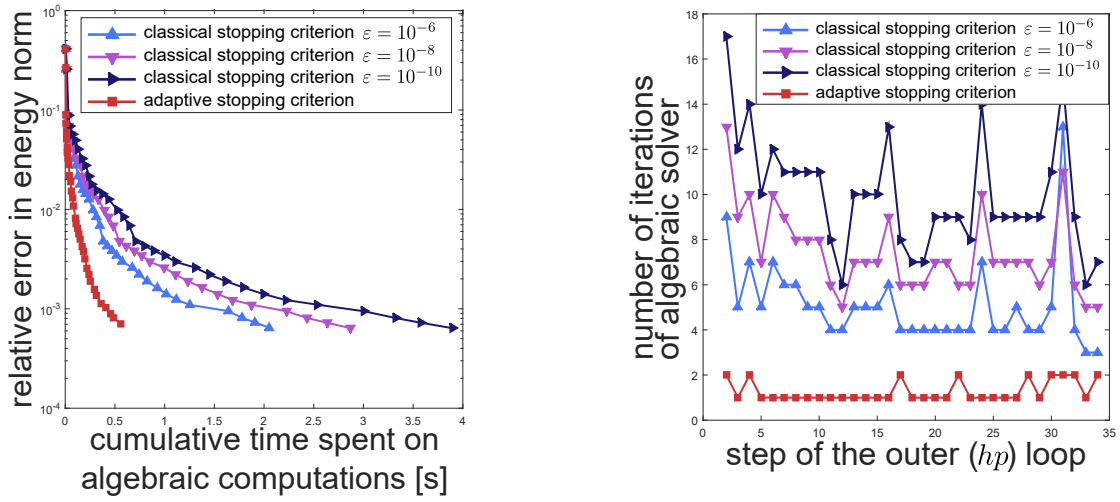

Figure 5: [Sharp-Gaussian of Section 6.1] Relative energy error $\|\nabla(u - u_\ell)\|/\|\nabla u\|$ as a function of cumulative time spent on algebraic computations with the stopping criteria (4.21) and (4.22) (*left*) and corresponding numbers of algebraic solver iterations per step of the inexact *hp*-adaptive algorithm described in Scheme 2 (*right*).

the mesh and polynomial-degree distribution obtained at the 17th step of the outer (hp) loop. On the right panel of Figure 6, we plot the corresponding inexact numerical solution obtained with the adaptive stopping criterion (4.21) for the algebraic solver, i.e. after the second V-cycle of the hp-multigrid solver. The detailed evolution of the total error lower bound (3.9) and algebraic error upper bound (3.6), the two

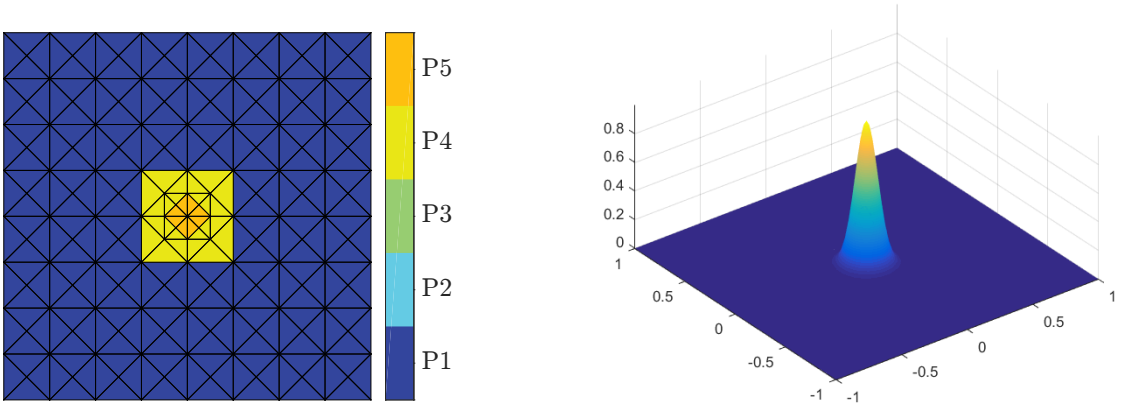

Figure 6: [Sharp-Gaussian of Section 6.1] Mesh and polynomial-degree distribution $(\mathcal{T}_{17}, \mathbf{p}_{17})$ (*left*) along with the corresponding numerical solution u_{17} obtained after 17 steps of the inexact hp-adaptive algorithm (*right*).

main ingredients for the stopping criterion (4.21), throughout the iterations of the algebraic solver at the 17th level of refinement is plotted on the left panel of Figure 7. The annotations in the left panel of Figure 7 illustrate that many additional (redundant) iterations of algebraic solver would be necessary in case of using the classical stopping criterion (4.22) with various values of the tolerance ε at this particular step of the outer (hp) loop with our stopping criterion (4.21). The corresponding values of the true algebraic error in comparison with the algebraic error upper bound, and the norm of the algebraic residual vector $\|\mathrm{R}_\ell\|$ are given on the right panel of Figure 7. We observe that the algebraic error upper bound, as well as the norm $\|\mathrm{R}_\ell\|$, closely follow the actual value of the algebraic error, with our error estimate giving a slightly tighter bound during the first three multigrid iterations. In Figure 8, left panel, we depict the total energy error along with its upper and lower bounds during the multigrid iterations. The quantitative evaluation of all the estimators computed within the module `ESTIMATE` in terms of their effectivity indices, i.e. the ratio of the estimates over the error for the upper bounds and the reciprocal for the lower bound, is given on the right panel of Figure 8. We note that also these effectivity indices take values close to the optimal value of one. The spatial distributions of the actual total and algebraic errors with the total upper error indicators and algebraic upper error indicators at the moment when the algebraic iterations are stopped on step $\ell = 17$ of the outer (hp) loop, as dictated by the adaptive stopping criterion (4.21), are displayed in Figures 9 and 10. We see that the actual and predicted error distributions match very nicely.

6.1.2 Strategy driven by the local Neumann problems

We also present the results obtained while employing within the inexact hp-adaptive algorithm the local residuals $r^{\mathbf{a},h}$ and $r^{\mathbf{a},p}$ defined via solving the local Neumann problems as proposed in Definitions 4.8 and 4.9. The use of these residuals leads to slightly different meshes and polynomial-degree distributions (not presented here for brevity). In particular, we plot the effectivity indices for the estimated reduction factor C_{red} and for the underlying lower bound $\underline{\eta}_{\mathcal{M}_\ell^\theta}$ in Figure 11. We find these estimates a little less precise compared to the ones presented in Figure 4, yet the effectivity indices are still quite close to one. The savings when using the adaptive stopping criterion (4.21) compared to the classical stopping criterion (4.22) are then demonstrated in Figure 12 in terms of the time spent on algebraic computations and in terms of the number of necessary iterations of the algebraic solver.

6.1.3 Exponential convergence

In Figure 13 we show that the proposed hp-refinement strategy (driven by solving either local Dirichlet problems or local Neumann problems) still leads, even in the presence of inexact solver, to meshes and

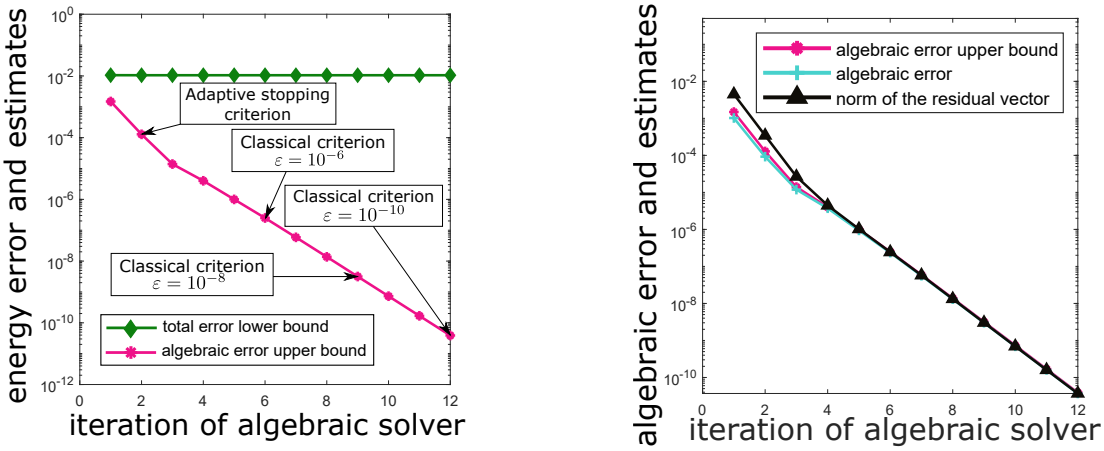

Figure 7: [Sharp-Gaussian of Section 6.1] Algebraic error upper bound $\eta_{\text{alg}}(u_{17}, \mathcal{T}_{17})$ compared with total error lower bound $\mu(u_{17})$ (*left*) and with true algebraic error $\|\nabla(u_{17}^{\text{ex}} - u_{17})\|$ and norm of algebraic residual vector $\|R_{17}\|$ (*right*) as a function of algebraic solver iterations. The annotations in the left panel indicate when the classical stopping criterion (4.22) with various values for the tolerance ε would be satisfied for this particular mesh.

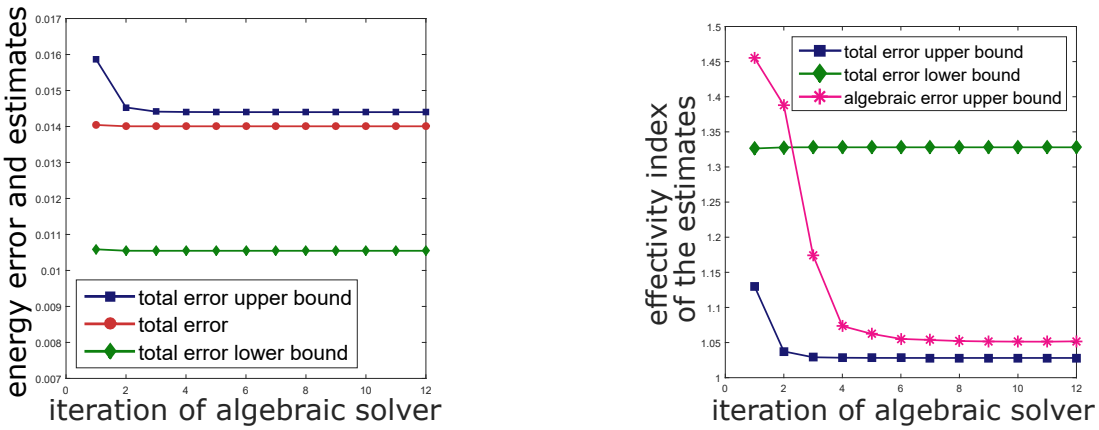

Figure 8: [Sharp-Gaussian of Section 6.1] Total energy error with its upper and lower bound (*left*) and effectivity indices for the total error upper bound (3.5), the total error lower bound (3.9), and the algebraic error upper bound (3.6) (*right*), throughout the iterations of the multigrid solver.

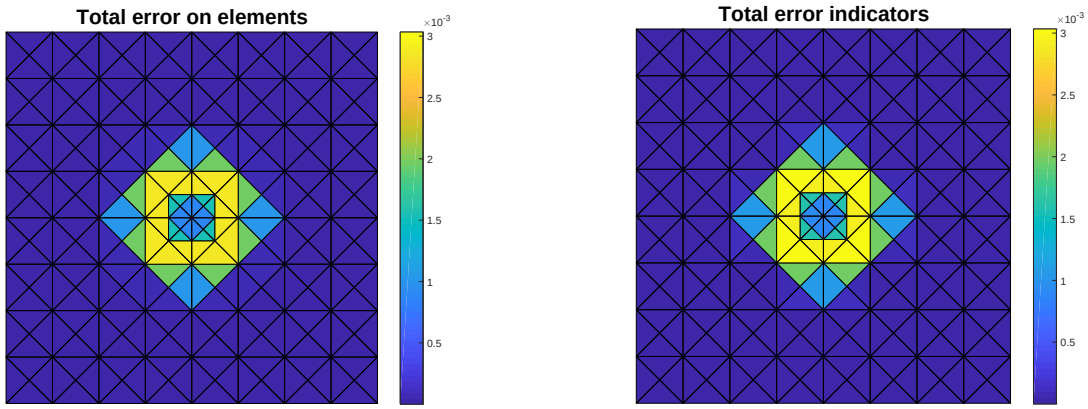

Figure 9: [Sharp-Gaussian of Section 6.1] Elementwise distribution of total energy error $\|\nabla(u - u_{17})\|$ (*left*) and total upper error indicators $\eta_K(u_{17})$ (*right*).

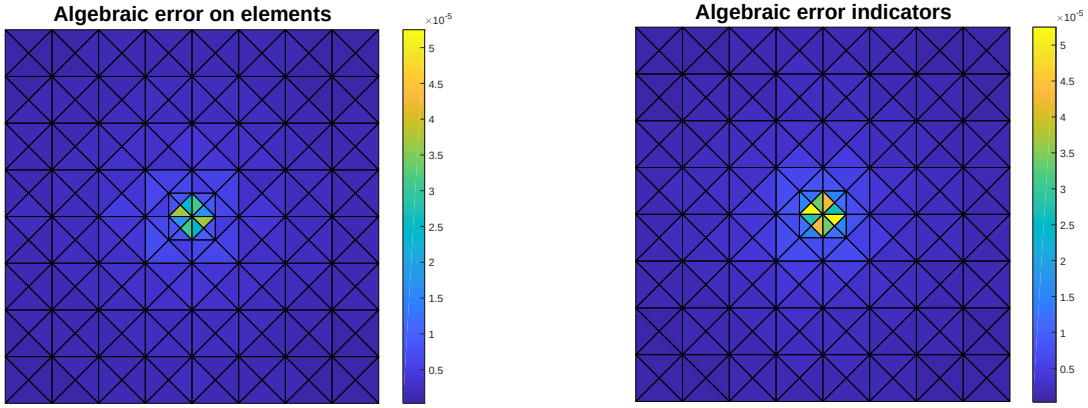

Figure 10: [Sharp-Gaussian of Section 6.1] Elementwise distribution of algebraic energy error $\|\nabla(u_{17}^{\mathrm{ex}} - u_{17})\|$ (*left*) and algebraic upper error indicators (*right*) using the adaptive stopping criterion (4.21) and $\gamma_{17} = 0.1$.

polynomial degree distributions for which the relative error decreases exponentially fast with respect to the number of degrees of freedom DoF_ℓ of the finite element spaces $\mathcal{V}_\ell$ in the form

$$\|\nabla(u - u_\ell)\| \leq C_1 \exp\left(-C_2 \mathrm{DoF}_\ell^{1/3}\right). \tag{6.3}$$

We plot the relative error $\|\nabla(u - u_\ell)\|/\|\nabla u\|$ as a function of $\mathrm{DoF}_\ell^{1/3}$ in logarithmic-linear scale for our strategy with inexact solver, the pure h-version of the outer loop with exact solver as given in Scheme 1, and while using the uniform h-refinement. We also plot the dashed line corresponding to expected form of exponential convergence (6.3) with $C_1 = 40.068$ and $C_2 = 1.033$ obtained by 2-parameter least squares fit of relative error decay observed while using our hp-refinement strategy (driven by solving local Dirichlet problems). For further comparison with different adaptive hp-refinement strategies (with exact algebraic solver) for this model problem, we refer to [15, Section 6.1].

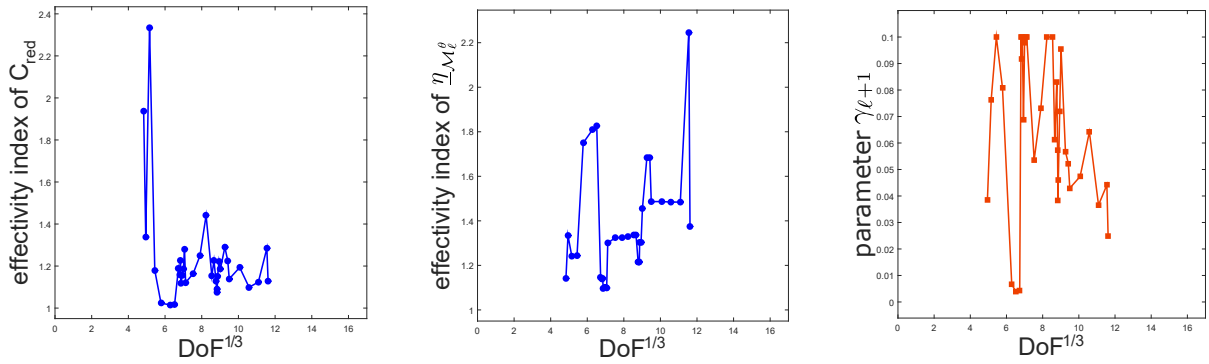

Figure 11: [Sharp-Gaussian of Section 6.1, strategy with local Neumann problems] Effectivity index for the error reduction factor estimate C_{red} of Theorem 5.4 (*left*); Effectivity index for the discrete lower bound $\underline{\eta}_{\mathcal{M}_\ell^\theta}$ of Lemma 5.2 given by (6.2) (*center*); corresponding values of parameter $\gamma_{\ell+1}$ used in (5.13) (*right*).

6.2 Smooth solution (asymmetric wave front)

Looking at the results of Section 6.1, namely Figures 5 and 12, one could be tempted to employ at each step of the outer (hp) loop only a single iteration of the algebraic solver with the hope to eventually converge to the correct solution, while saving a substantial amount of computational effort. This kind of heuristic approach may actually be beneficial in cases where we launch the inexact hp-adaptive algorithm with a good enough initial guess. However, as we demonstrate here in a fabricated setting, in case of an inaccurate initial guess, it is the present adaptive strategy that represents a safe choice, while outperforming both the heuristic approach and the adaptive strategies with algebraic solver piloted by classical stopping criteria.

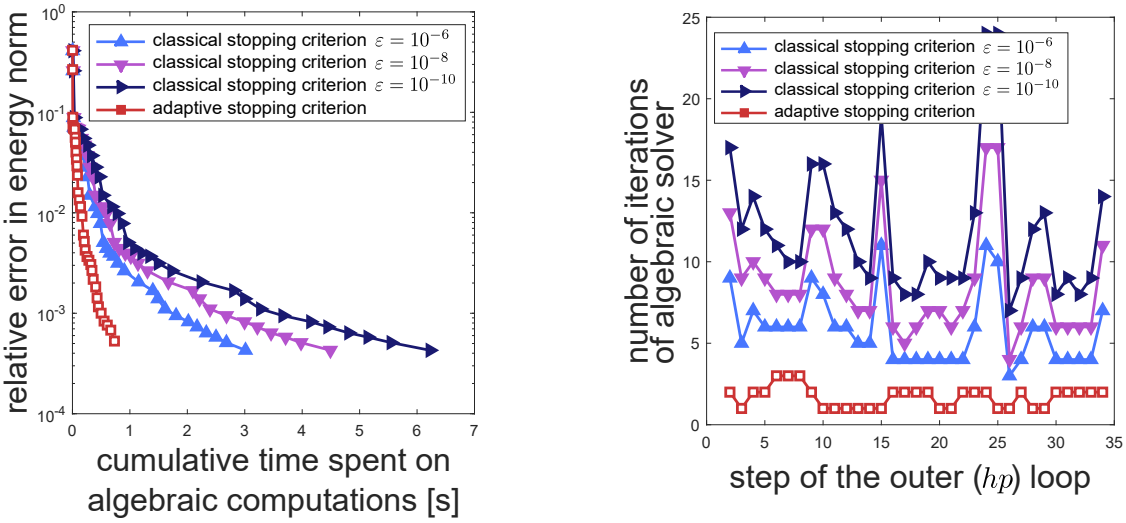

Figure 12: [Sharp-Gaussian of Section 6.1, strategy with local Neumann problems] Relative energy error $\|\nabla(u - u_\ell)\|/\|\nabla u\|$ as a function of cumulative time spent on algebraic computations with the stopping criteria (4.21) and (4.22) (*left*) and corresponding numbers of algebraic solver iterations per step of the outer (hp) loop. (*right*).

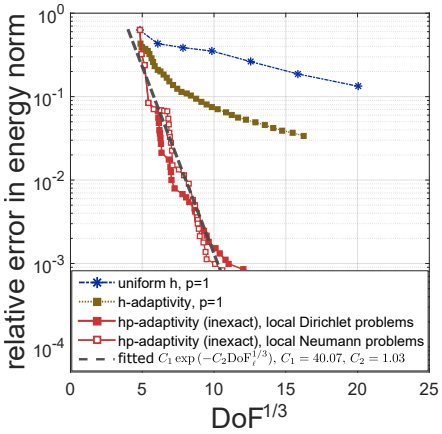

Figure 13: [Sharp-Gaussian of Section 6.1] Relative energy error $\|\nabla(u-u_\ell)\|/\|\nabla u\|$ as a function of $\mathrm{DoF}_\ell^{\frac{1}{3}}$, obtained with our hp-refinement strategy (driven by solving local Dirichlet problems and also local Neumann problems) with inexact algebraic solver, purely h-adaptive version with exact solver and using uniform h-refinement. The dashed line corresponds to (6.3) with constants obtained by fitting the error decay obtained with the present inexact hp-adaptive algorithm (driven by solving local Dirichlet problems).

To illustrate our point, we consider as the second test case a problem posed on the square domain $\Omega := (0,1) \times (0,1)$ with the exact solution (in polar coordinates)

$$u(r) = \arctan\left(\alpha(r - r_0)\right), \quad r = \sqrt{(x - x_\mathrm{c})^2 + (y - y_\mathrm{c})^2}$$

containing a wave front asymmetric within the domain. The parameter $\alpha := 100$ prescribes the steepness of the circular wave front with radius $r_0 := 0.92$ centered at the point $(x_\mathrm{c}, y_\mathrm{c}) := (1.5, 0.25)$, see Figure 14 (left panel) (for other variants of the wave front problem, we refer to Mitchell and McClain [34, Sections 5.16–5.19]). For this test case and also the test case of Section 6.3, the total error upper bound $\eta(u_\ell, \mathcal{T}_\ell)$ employed within the inexact hp-adaptive algorithm takes into account the error from the approximation of the inhomogeneous Dirichlet boundary condition prescribed by the exact solution on $\partial\Omega$; to this purpose, we proceed as described in [16, Theorem 3.3] and the references therein.

We start the computation with a criss-cross grid $\mathcal{T}_0$ with $\max_{K \in \mathcal{T}_0} h_K = 0.125$. In contrast to the other test cases and the description of the module `ONE_SOLVER_STEP` in Section 4.1, this time we solve the

algebraic system inexactly even at the initial level $\ell = 0$ using a geometric V-cycle multigrid solver with a hierarchy of 4 additional meshes obtained by uniform coarsening of the mesh $\mathcal{T}_0$. As the initial guess for the algebraic solver, we consider a vector corresponding to a function which poorly approximates the wave front since it contains a peak in the region where the exact solution is essentially flat. We display the contour plot of the initial guess function in the right panel of Figure 14. In the left panel of Figure 15, we plot the obtained mesh and polynomial degree distribution $(\mathcal{T}_{20}, \mathbf{p}_{20})$ after 20 steps of the outer (hp) loop driven by solving local Neumann problems (Definitions 4.8 and 4.9) and when employing the so-called heuristic approach, i.e. performing only a single iteration of the algebraic solver at each level of refinement. Note the extra refinements present in the region of the peak of the initial guess function: these are not present when employing the adaptive stopping criterion (4.21) for the algebraic solver, see the right panel of Figure 15. Figure 16 shows the spatial distribution of the actual total error and the total upper error indicators corresponding to $(\mathcal{T}_{20}, \mathbf{p}_{20})$ from Figure 15 (right panel) at the moment when the algebraic solver is stopped using (4.21) with $\gamma_{20} = 0.1$. Moreover, Figure 17 presents the comparison of different stopping criteria for the algebraic solver in terms of the number of necessary algebraic iterations per iteration of the outer (hp) loop, and in terms of the amount of time spent on the algebraic computations in order to reach a relative estimated error lower than 0.01. We observe that while using the heuristic approach, compared to the use of the adaptive stopping criterion, nine additional iterations of the outer (hp) loop were necessary (due to incorrect refinements at the beginning of the adaptive process). Even though only one single iteration is performed per each step of the outer (hp) loop, we altogether spend approximately 4 times more time on algebraic computations than in the case of using adaptive stopping criterion. The heuristic approach surprisingly turns out to be comparable with the use of the classical criterion with $\varepsilon = 10^{-6}$ in this overall cost assessment. Then, Figure 18 presents the effectivity indices for the reduction factor C_{red} and the lower bound $\underline{\eta}_{\mathcal{M}_\ell^\theta}$; both indices are quite promising even for this test case. The value $\gamma_\ell = 0.1$ is used throughout the whole inexact hp-adaptive algorithm. Lastly, Figure 19 shows the error decay with respect to $\mathrm{DoF}_\ell^{\frac{1}{3}}$ when using the proposed strategy with inexact algebraic solver and, for comparison, also while using a pure h-adaptive version of the loop given by Scheme 1, and using simply uniform h-refinement. We observe that also for this model problem, the proposed strategy leads to an exponential convergence rate; the corresponding values of the constants C_1 and C_2 in the expression (6.3) obtained by a 2-parameter least-squares fit are 3.952 and 0.325, respectively.

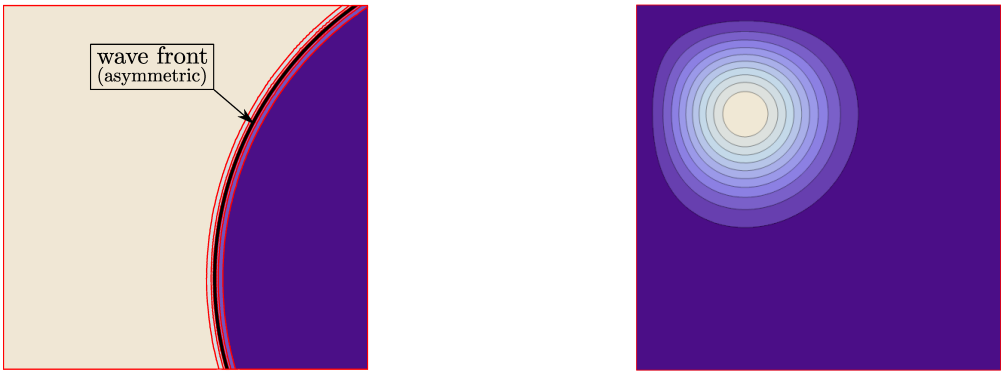

Figure 14: [Asymmetric wave front of Section 6.2] Contour plots of exact solution (*left*) and function inducing the initial guess for the algebraic solver (*right*).

6.3 Singular solution (L-shape domain)

As a model problem with singular exact solution, we consider the classic re-entrant corner problem, cf. [34, 16, 15], posed on the L-shape domain $\Omega = (-1,1) \times (-1,1) \setminus [0,1] \times [-1,0]$ with $f = 0$ and the weak solution (in polar coordinates)

$$u(r,\varphi) = r^{\frac{2}{3}} \sin\left(\frac{2\varphi}{3}\right).$$

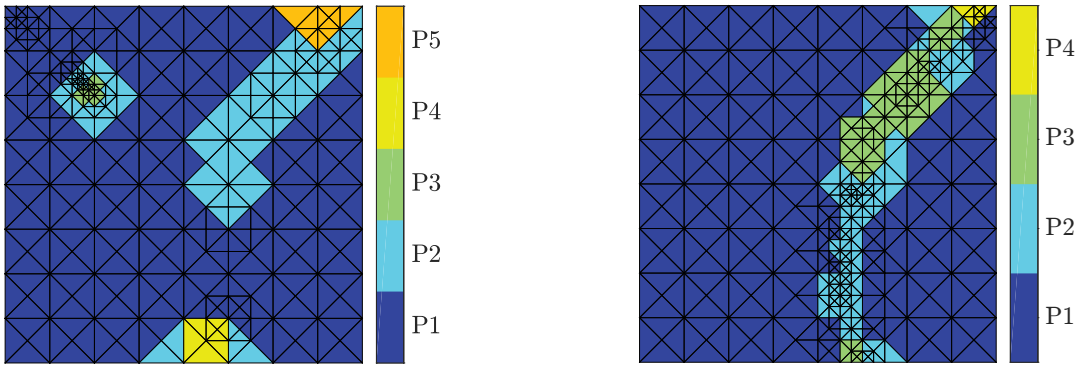

Figure 15: [Asymmetric wave front of Section 6.2] Mesh and polynomial degree distribution $(\mathcal{T}_{20}, \mathbf{p}_{20})$ obtained using the so-called heuristic approach (one multigrid iteration on each step of the outer (hp) loop) (*left*) and employing the adaptive stopping criterion (4.21) (*right*).

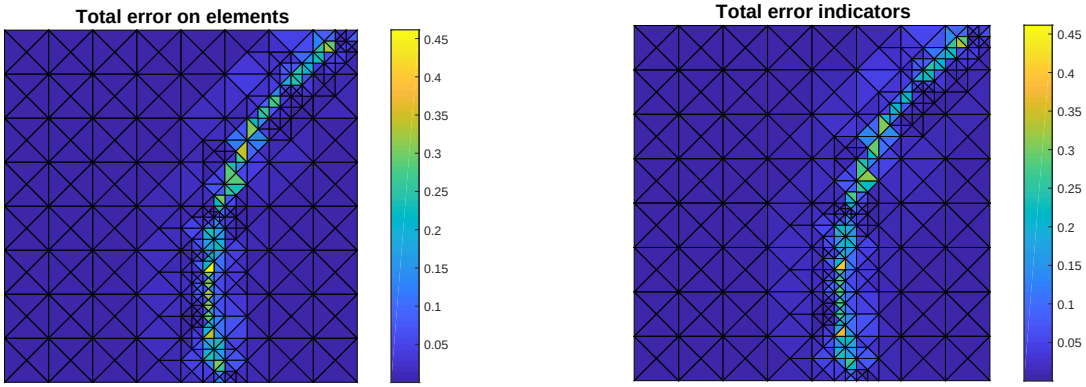

Figure 16: [Asymmetric wave front of Section 6.2] Elementwise distribution of total energy error $\|\nabla(u - u_{20})\|$ (*left*) and total upper error indicators $\eta_K(u_{20})$ (*right*). The effectivity index for the estimate is 1.1106.

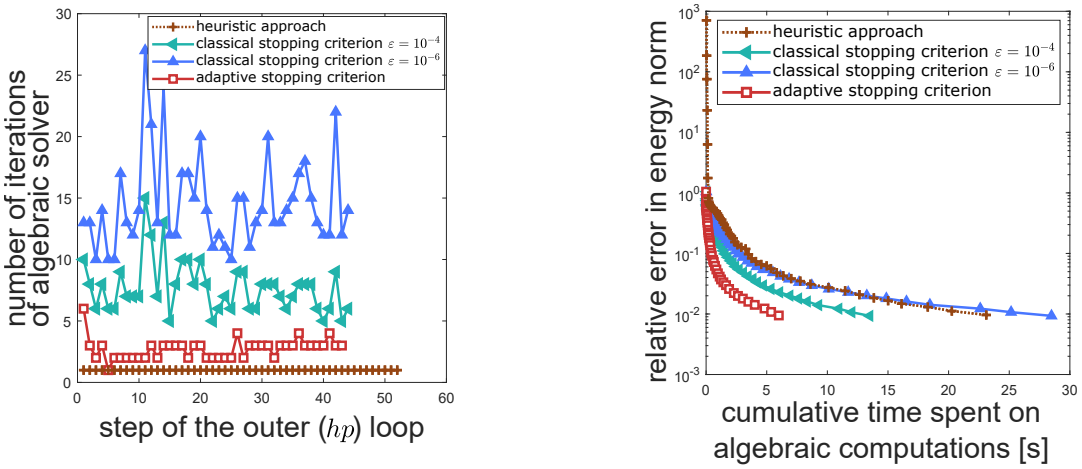

Figure 17: [Asymmetric wave front of Section 6.2] Relative energy error $\|\nabla(u - u_\ell)\|/\|\nabla u\|$ as a function of cumulative time spent on algebraic computations for the various stopping criteria of Section 4.3 (*left*) and corresponding numbers of algebraic solver iterations per step of the outer (hp) loop. (*right*).

We start the computation on a coarse criss-cross grid $\mathcal{T}_0$ with $\max_{K\in\mathcal{T}_0} h_K = 0.25$ and all the polynomial degrees set uniformly to 1. We present here the results obtained with our strategy driven by solving the local Dirichlet problems. We note that the results obtained with the strategy employing the local residuals

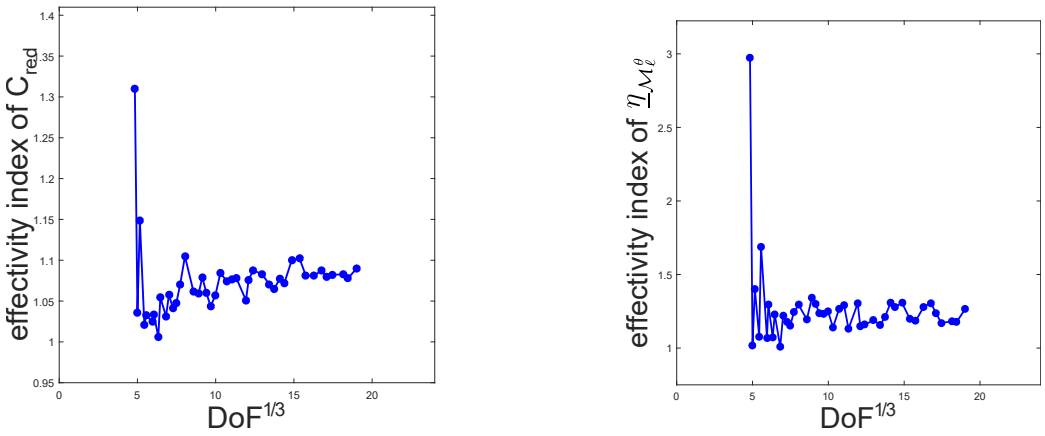

Figure 18: [Asymmetric wave front of Section 6.2] Effectivity indices for the error reduction factor estimate $C_{\rm red}$ of Theorem 5.4 given by (6.1) (*left*) and the discrete lower bound $\underline{\eta}_{\mathcal{M}_\ell^\theta}$ of Lemma 5.2 given by (6.2) (*right*).

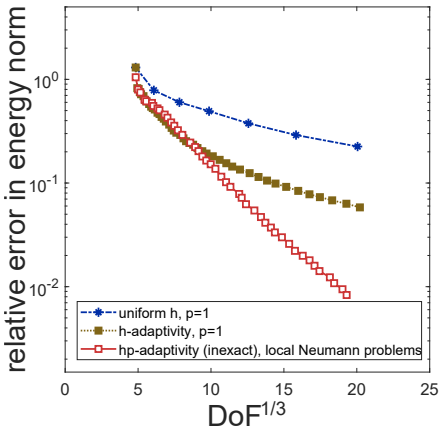

Figure 19: [Asymmetric wave front of Section 6.2] Relative energy error $\|\nabla(u-u_\ell)\|/\|\nabla u\|$ as a function of $\mathrm{DoF}_\ell^{\frac{1}{3}}$, obtained with the present inexact *hp*-adaptive algorithm (driven by solving local Neumann problems) with inexact algebraic solver, purely *h*-adaptive version with exact solver and using uniform *h*-refinement.

$r^{\mathbf{a},h}$ and $r^{\mathbf{a},p}$ from Definitions 4.8 and 4.9 are very similar. Owing to the corner singularity, we employ a Dunavant quadrature with 400 points to compute the actual error on the simplices around the corner.

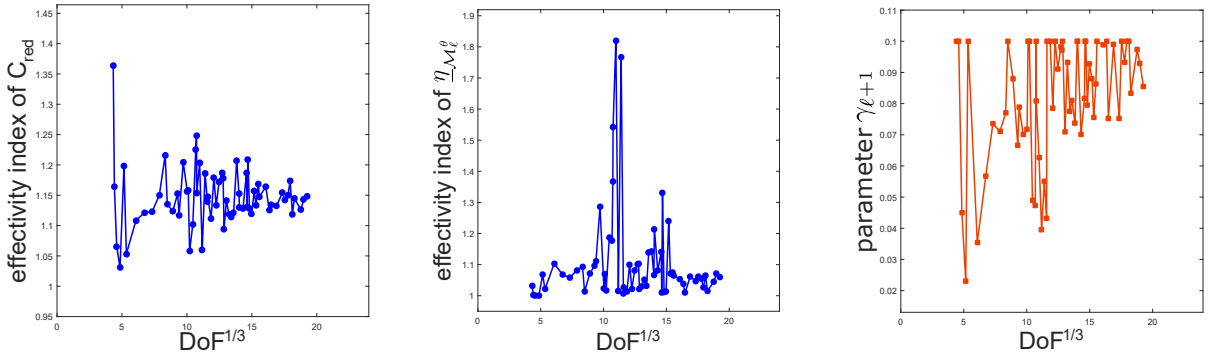

Figure 20: [L-shape domain of Section 6.3] Effectivity index for the error reduction factor estimate $C_{\rm red}$ of Theorem 5.4 given by (6.1) (*left*); Effectivity index for the discrete lower bound $\underline{\eta}_{\mathcal{M}_\ell^\theta}$ of Lemma 5.1 given by (6.2) (*center*); corresponding values of the parameter $\gamma_{\ell+1}$ used in (5.13) (*right*).

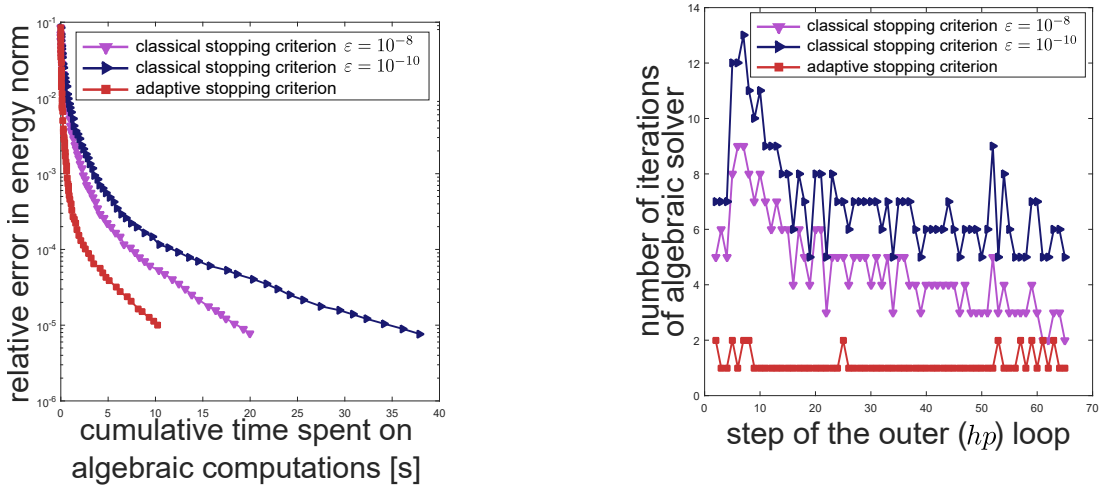

Figure 21: [L-shape domain of Section 6.3] Relative energy error $\|\nabla(u - u_\ell)\|/\|\nabla u\|$ as a function of cumulative time spent on algebraic computations for the various stopping criteria of Section 4.3 (*left*) and respective numbers of algebraic solver iterations per step of the outer (hp) loop. (*right*).

First, in Figure 20, we assess the quality of the estimated reduction factor $C_{\rm red}$ and the lower bound $\underline{\eta}_{\mathcal{M}_\ell^\theta}$. We observe that the effectivity indices remain close to the optimal value of one also for this test case. In the right panel of Figure 20, we plot the corresponding values of the parameter $\gamma_{\ell+1}$ used within the stopping criterion (5.11). Next, Figure 21 demonstrates how the use of the stopping criterion (5.11) allows one to cut off the unnecessary iterations of the multigrid solver and save a substantial portion of the computational time spent on algebraic computations. Using the multigrid solver controlled by (5.11), to reach the relative error lower than 10^{-5}, one saves about 50%, or even 75%, of the computational time dedicated to the algebraic solver in case of the use of the classical stopping criterion (4.22) with $\varepsilon = 10^{-8}$ or $\varepsilon = 10^{-10}$, respectively. In the left panel of Figure 22, we investigate the evolution of the total error lower bound (3.9) and the algebraic error upper bound (3.6) throughout the iterations of the multigrid solver at the 7th level of refinement (obtained while employing the adaptive stopping criterion (5.11) on all the previous steps of the outer (hp) loop). The annotations in the left panel illustrate that many additional (redundant) iterations of algebraic solver would be necessary in case of using the classical stopping criterion (4.22) with the tolerances $\varepsilon = 10^{-8}$ and $\varepsilon = 10^{-10}$ at this particular step of the outer (hp) loop with our stopping criterion (4.21). The quality of all the error bounds computed within the `ESTIMATE` module, at the same level of refinement, can be appreciated in the right panel of Figure 22. The corresponding mesh and polynomial degree distribution $(\mathcal{T}_7, \mathbf{p}_7)$ is displayed in the left panel of Figure 23. In Figure 23 (central and right panels) and Figure 24, we show the spatial distribution of the actual total and algebraic errors along with the total upper error indicators and algebraic upper error indicators after the 2nd iteration of multigrid solver on the 7th step of the outer (hp) loop, i.e. at the moment when we stopped the multigrid solver as dictated by the adaptive stopping criterion (4.21). To conclude, we display in Figure 25 the overall decay of the relative error as a function of $\mathrm{DoF}_\ell^{\frac{1}{3}}$ in logarithmic-linear scale, to illustrate that also for this problem with singular exact solution, the present inexact hp-adaptive algorithm leads to an asymptotic exponential convergence rate; for this test case, the corresponding values of C_1 and C_2 in the expression (6.3) obtained by a 2-parameter least-squares fit are 4.357 and 0.679, respectively. We also display the results obtained with uniform h-refinement, with a pure h-version of the adaptive loop from Scheme 1, and the hp-adaptation based on a priori knowledge of the weak solution, inspired by the theoretical results for the one-dimensional problem with singular solution [1, 2, 35], leading (to our knowledge) to the best convergence rate. For further comparison with some other hp-refinement strategies (with exact algebraic solver), we refer to [15, Section 6.2], [34, Section 5.4].

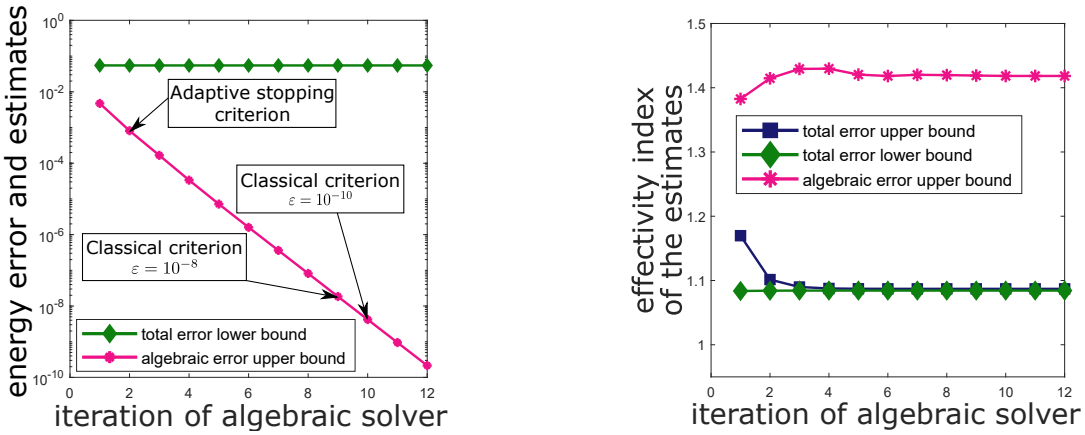

Figure 22: [L-shape domain of Section 6.3] Algebraic error upper bound $\eta_{\mathrm{alg}}(u_7, \mathcal{T}_7)$ compared with total error lower bound $\mu(u_7)$ (*left*); effectivity indices for the total error upper bound (3.5), the total error lower bound (3.9), and the algebraic error upper bound (3.6) (*right*), throughout the iterations of the multigrid solver. The annotations in the left panel indicate when the classical stopping criterion (4.22) with the tolerances $\varepsilon = 10^{-8}$ and $\varepsilon = 10^{-10}$ would be satisfied for this particular mesh.

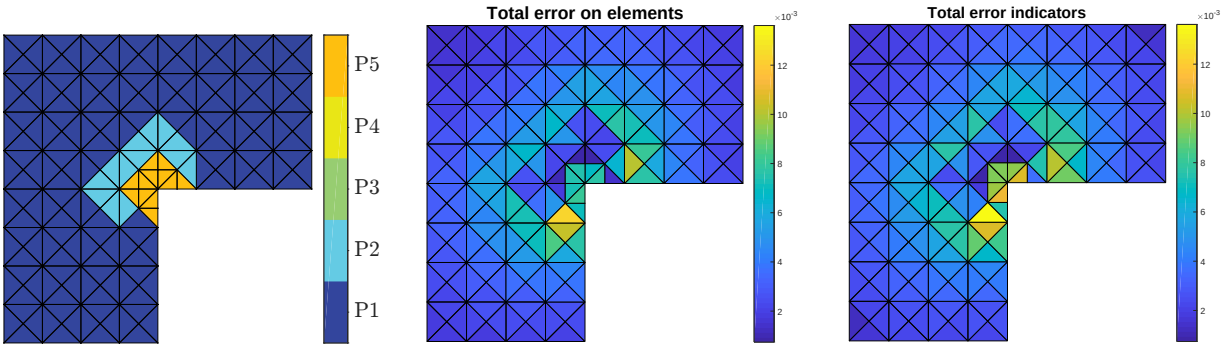

Figure 23: [L-shape domain of Section 6.3] Mesh and polynomial degree distribution $(\mathcal{T}_7, \mathbf{p}_7)$; corresponding elementwise distribution of the total energy error $\|\nabla(u - u_7)\|$ (*left*) and total error indicators $\eta_K(u_7)$ (*right*).

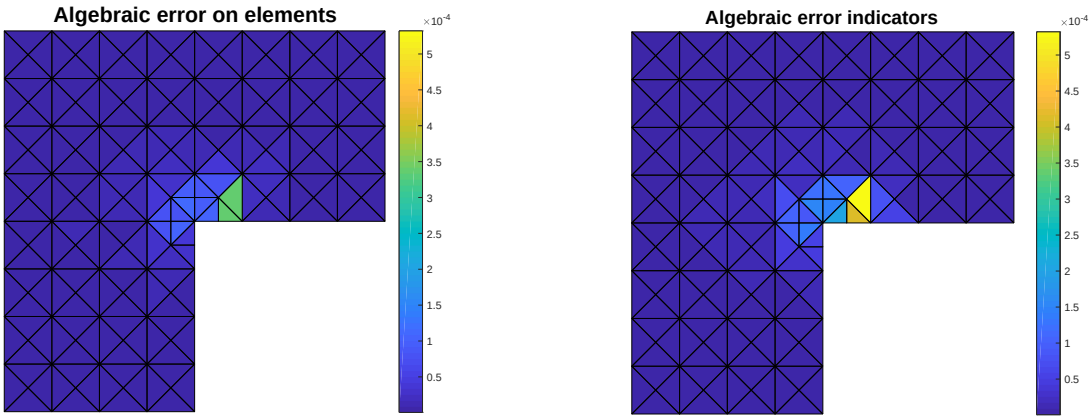

Figure 24: [L-shape domain of Section 6.3] Elementwise distribution of the algebraic energy error $\|\nabla(u_7^{\mathrm{ex}} - u_7)\|$ (*left*) and algebraic error indicators $\eta_{\mathrm{alg},K}(u_7)$ (*right*) obtained using the adaptive stopping criterion (4.21) with $\gamma_\ell = 0.04$.

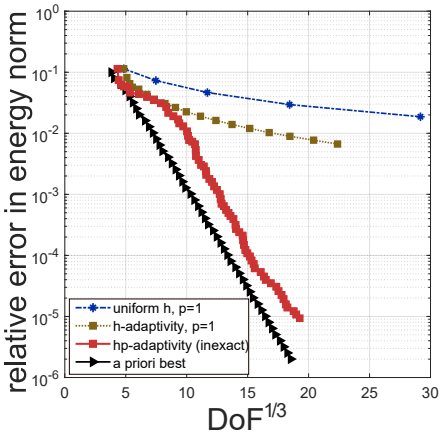

Figure 25: [L-shape domain of Section 6.3] Relative energy error $\|\nabla(u-u_\ell)\|/\|\nabla u\|$ as a function of $\mathrm{DoF}_\ell^{\frac{1}{3}}$, obtained with the present inexact *hp*-adaptive algorithm (driven by solving local Dirichlet problems) with inexact algebraic solver, using uniform *h*-refinement, purely *h*-adaptive version of the adaptive loop in Scheme 1, and its *hp*-version exploiting the a priori knowledge of the weak solution.

7 Conclusions

In this work, we extended our adaptive *hp*-refinement strategy for solving elliptic problems by taking into account an inexact algebraic solver within the outer (*hp*) loop and driving this inexact algebraic solver adaptively. We constructed flux reconstructions and a total residual lifting by solving small local problems on patches of elements, yielding guaranteed a posteriori error bounds on algebraic and total errors. Then we proposed a stopping criterion for the iterative algebraic solver ensuring the desired balance between the algebraic and the total error at each outer (*hp*) loop step. The total error indicators are employed to mark mesh vertices, whereas the actual *hp*-refinement decision is driven by solving additional local problems on the patches of elements associated with the marked vertices. Once the next mesh and polynomial degree distribution have been determined, solving one additional local problem per marked vertex leads to a fully computable guaranteed bound on the error reduction factor between two successive inexact approximations. We considered here two options for the local problems on patches around marked vertices, with homogeneous Dirichlet and homogeneous Neumann boundary conditions.

The local problems form a distinctive feature at the heart of our approach. Their size is limited and they are intrinsically parallel since they are mutually independent. Their inclusion, on the other hand, involves a coding effort as well as a resolution effort at each (inner and outer) step, so that the resulting *hp* strategy is likely to be more expensive than some other (local) *hp*-refinement strategies. We believe, though, that this is a reasonable price to pay to achieve all the described benefits.

The numerical experiments demonstrate the accuracy of the estimated quantities while highlighting the applicability of the presented strategy. For all the test cases, the obtained meshes and polynomial degree distributions lead to asymptotic exponential convergence rates. A further theoretical analysis of the reduction factor C_{red} still constitutes a relevant topic of research, as indicated in Remark 5.6.

The present approach extends easily to inhomogeneous Dirichlet and Neumann conditions and full-matrix anisotropic and inhomogeneous diffusion tensor, as in [16]. The approach can also be rather straightforwardly extended to sign-changing diffusion tensors, linear elasticity, eigenvalue problems, singularly-perturbed reaction–diffusion problems, Stokes problem, Leray–Lions nonlinear diffusion problems, and for estimates of the error in a quantity of interest, see among others [36, 37, 38, 39] for a few selected references. Extensions to the parabolic heat equation would also be possible following [40]. The most challenging limitations of the present methodology are from our viewpoint singularly perturbed advection-diffusion equations and more complicated (unsteady) nonlinear problems.

References

[1] W. Gui, I. Babuška, The h, p and h-p versions of the finite element method in 1 dimension. II. The error analysis of the h- and h-p versions, Numer. Math. 49 (6) (1986) 613–657. doi:10.1007/BF01389734.
URL http://dx.doi.org/10.1007/BF01389734

[2] W. Gui, I. Babuška, The h, p and h-p versions of the finite element method in 1 dimension. III. The adaptive h-p version, Numer. Math. 49 (6) (1986) 659–683. doi:10.1007/BF01389735.
URL http://dx.doi.org/10.1007/BF01389735

[3] I. Babuška, B. Guo, The h-p version of finite element method, part 1: The basic approximation results, Comp. Mech. (1) (1986) 21–41.

[4] I. Babuška, B. Guo, The h-p version of finite element method, part 2: General results and application, Comp. Mech. (1) (1986) 203–220.

[5] R. H. Nochetto, K. G. Siebert, A. Veeser, Theory of adaptive finite element methods: an introduction, in: Multiscale, nonlinear and adaptive approximation, Springer, Berlin, 2009, pp. 409–542. doi:10.1007/978-3-642-03413-8_12.
URL http://dx.doi.org/10.1007/978-3-642-03413-8_12

[6] R. Stevenson, An optimal adaptive finite element method, SIAM J. Numer. Anal. 42 (5) (2005) 2188–2217. doi:10.1137/S0036142903425082.
URL http://dx.doi.org/10.1137/S0036142903425082

[7] R. Stevenson, Optimality of a standard adaptive finite element method, Found. Comput. Math. 7 (2) (2007) 245–269. doi:10.1007/s10208-005-0183-0.
URL http://dx.doi.org/10.1007/s10208-005-0183-0

[8] M. Arioli, E. H. Georgoulis, D. Loghin, Stopping criteria for adaptive finite element solvers, SIAM J. Sci. Comput. 35 (3) (2013) A1537–A1559. doi:10.1137/120867421.
URL http://dx.doi.org/10.1137/120867421

[9] M. Arioli, J. Liesen, A. Międlar, Z. Strakoš, Interplay between discretization and algebraic computation in adaptive numerical solution of elliptic PDE problems, GAMM-Mitt. 36 (1) (2013) 102–129. doi:10.1002/gamm.201310006.
URL http://dx.doi.org/10.1002/gamm.201310006

[10] M. Holst, R. Szypowski, Y. Zhu, Adaptive finite element methods with inexact solvers for the nonlinear Poisson-Boltzmann equation, in: Domain decomposition methods in science and engineering XX, Vol. 91 of Lect. Notes Comput. Sci. Eng., Springer, Heidelberg, 2013, pp. 167–174. doi:10.1007/978-3-642-35275-1.
URL https://doi.org/10.1007/978-3-642-35275-1

[11] C. Carstensen, M. Feischl, M. Page, D. Praetorius, Axioms of adaptivity, Comput. Math. Appl. 67 (6) (2014) 1195–1253. doi:10.1016/j.camwa.2013.12.003.
URL http://dx.doi.org/10.1016/j.camwa.2013.12.003

[12] G. Gantner, A. Haberl, D. Praetorius, B. Stiftner, Rate optimal adaptive FEM with inexact solver for nonlinear operators, IMA J. Numer. Anal.DOI 10.1093/imanum/drx050 (2017). doi:10.1093/imanum/drx050.

[13] R. Becker, C. Johnson, R. Rannacher, Adaptive error control for multigrid finite element methods, Computing 55 (4) (1995) 271–288. doi:10.1007/BF02238483.
URL http://dx.doi.org/10.1007/BF02238483

[14] A. Ern, M. Vohralík, Adaptive inexact Newton methods with a posteriori stopping criteria for nonlinear diffusion PDEs, SIAM J. Sci. Comput. 35 (4) (2013) A1761–A1791. doi:10.1137/120896918.
URL http://dx.doi.org/10.1137/120896918

[15] P. Daniel, A. Ern, I. Smears, M. Vohralík, An adaptive hp-refinement strategy with computable guaranteed bound on the error reduction factor, Computers and Mathematics with ApplicationsHttps://doi.org/10.1016/j.camwa.2018.05.034 (2018). doi:https://doi.org/10.1016/j.camwa.2018.05.034.
URL http://www.sciencedirect.com/science/article/pii/S0898122118303109

[16] V. Dolejší, A. Ern, M. Vohralík, hp-adaptation driven by polynomial-degree-robust a posteriori error estimates for elliptic problems, SIAM J. Sci. Comput. 38 (5) (2016) A3220–A3246. doi:10.1137/15M1026687.
URL http://dx.doi.org/10.1137/15M1026687

[17] J. Papež, U. Rüde, M. Vohralík, B. Wohlmuth, Sharp algebraic and total a posteriori error bounds for h and p finite elements via a multilevel approach, HAL preprint 01662944 (2017).
URL https://hal.inria.fr/hal-01662944

[18] W. Dörfler, A convergent adaptive algorithm for Poisson's equation, SIAM J. Numer. Anal. 33 (3) (1996) 1106–1124. doi:10.1137/0733054.
URL http://dx.doi.org/10.1137/0733054

[19] J. Papež, Z. Strakoš, M. Vohralík, Estimating and localizing the algebraic and total numerical errors using flux reconstructions, Numer. Math. 138 (3) (2018) 681–721. doi:10.1007/s00211-017-0915-5.
URL https://doi.org/10.1007/s00211-017-0915-5

[20] P. Destuynder, B. Métivet, Explicit error bounds in a conforming finite element method, Math. Comp. 68 (228) (1999) 1379–1396. doi:10.1090/S0025-5718-99-01093-5.
URL http://dx.doi.org/10.1090/S0025-5718-99-01093-5

[21] D. Braess, V. Pillwein, J. Schöberl, Equilibrated residual error estimates are p-robust, Comput. Methods Appl. Mech. Engrg. 198 (13-14) (2009) 1189–1197.

[22] A. Ern, M. Vohralík, Polynomial-degree-robust a posteriori estimates in a unified setting for conforming, nonconforming, discontinuous Galerkin, and mixed discretizations, SIAM J. Numer. Anal. 53 (2) (2015) 1058–1081. doi:10.1137/130950100.
URL http://dx.doi.org/10.1137/130950100

[23] A. Ern, M. Vohralík, Stable broken H^1 and $\mathbf{H}(\mathrm{div})$ polynomial extensions for polynomial-degree-robust potential and flux reconstruction in three space dimensions, HAL Preprint 01422204 (2016).

[24] P. Jiránek, Z. Strakoš, M. Vohralík, A posteriori error estimates including algebraic error and stopping criteria for iterative solvers, SIAM J. Sci. Comput. 32 (3) (2010) 1567–1590. doi:10.1137/08073706X.
URL http://dx.doi.org/10.1137/08073706X

[25] V. Rey, C. Rey, P. Gosselet, A strict error bound with separated contributions of the discretization and of the iterative solver in non-overlapping domain decomposition methods, Comput. Methods Appl. Mech. Engrg. 270 (2014) 293–303. doi:10.1016/j.cma.2013.12.001.
URL http://dx.doi.org/10.1016/j.cma.2013.12.001

[26] I. Babuška, T. Strouboulis, The finite element method and its reliability, Numerical Mathematics and Scientific Computation, The Clarendon Press Oxford University Press, New York, 2001.

[27] S. I. Repin, A posteriori estimates for partial differential equations, Vol. 4 of Radon Series on Computational and Applied Mathematics, Walter de Gruyter GmbH & Co. KG, Berlin, 2008.

[28] F. Brezzi, M. Fortin, Mixed and hybrid finite element methods, Vol. 15 of Springer Series in Computational Mathematics, Springer-Verlag, New York, 1991. doi:10.1007/978-1-4612-3172-1.
URL http://dx.doi.org/10.1007/978-1-4612-3172-1

[29] J. E. Roberts, J.-M. Thomas, Mixed and hybrid methods, in: Handbook of Numerical Analysis, Vol. II, North-Holland, Amsterdam, 1991, pp. 523–639.

[30] E. G. Sewell, Automatic generation of triangulations for piecewise polynomial approximation, ProQuest LLC, Ann Arbor, MI, 1972, thesis (Ph.D.)–Purdue University.

[31] W. F. Mitchell, A comparison of adaptive refinement techniques for elliptic problems, ACM Trans. Math. Software 15 (4) (1989) 326–347 (1990). doi:10.1145/76909.76912.
URL http://dx.doi.org/10.1145/76909.76912

[32] P. Morin, R. H. Nochetto, K. G. Siebert, Convergence of adaptive finite element methods, SIAM Rev. 44 (4) (2002) 631–658 (2003), revised reprint of "Data oscillation and convergence of adaptive FEM" [SIAM J. Numer. Anal. 38 (2000), no. 2, 466–488; MR1770058 (2001g:65157)]. doi:10.1137/S0036144502409093.
URL http://dx.doi.org/10.1137/S0036144502409093

[33] R. Verfürth, A posteriori error estimation techniques for finite element methods, Numerical Mathematics and Scientific Computation, Oxford University Press, Oxford, 2013. doi:10.1093/acprof:oso/9780199679423.001.0001.
URL http://dx.doi.org/10.1093/acprof:oso/9780199679423.001.0001

[34] W. F. Mitchell, M. A. McClain, A comparison of hp-adaptive strategies for elliptic partial differential equations (long version), NISTIR 7824, National Institute of Standards and Technology (2011).
URL https://math.nist.gov/~WMitchell/papers/nistir7824.pdf

[35] B. Szabó, I. Babuška, Finite element analysis, A Wiley-Interscience Publication, John Wiley & Sons Inc., New York, 1991.

[36] P. Ciarlet, Jr., M. Vohralík, Localization of global norms and robust a posteriori error control for transmission problems with sign-changing coefficients, M2AN Math. Model. Numer. Anal. 52 (5) (2018) 2037–2064. doi:10.1051/m2an/2018034.
URL https://doi.org/10.1051/m2an/2018034

[37] E. Cancès, G. Dusson, Y. Maday, B. Stamm, M. Vohralík, Guaranteed and robust a posteriori bounds for Laplace eigenvalues and eigenvectors: conforming approximations, SIAM J. Numer. Anal. 55 (5) (2017) 2228–2254. doi:10.1137/15M1038633.
URL http://dx.doi.org/10.1137/15M1038633

[38] I. Smears, M. Vohralík, Simple and robust equilibrated flux a posteriori estimates for singularly perturbed reaction–diffusion problems, HAL Preprint 01956180, submitted for publication (2018).
URL https://hal.inria.fr/hal-01956180

[39] G. Mallik, M. Vohralík, S. Yousef, Goal-oriented a posteriori error estimation for conforming and nonconforming approximations with inexact solvers, HAL Preprint 01964733, submitted for publication (2018).
URL https://hal.inria.fr/hal-01964733

[40] A. Ern, I. Smears, M. Vohralík, Guaranteed, locally space-time efficient, and polynomial-degree robust a posteriori error estimates for high-order discretizations of parabolic problems, SIAM J. Numer. Anal. 55 (6) (2017) 2811–2834. doi:10.1137/16M1097626.
URL https://doi.org/10.1137/16M1097626